Hippeastrum hybridum assisted bioreduction of Hydrogen tetrachloroaurate (III) trihydrate: Multifaced application

Naila Sher
Mushtaq Ahmed (mushtaq213@yahoo.com)
University of Science and Technology Bannu https://orcid.org/0000-0002-0286-326X
Nadia Mushtaq
Rahmat Ali Khan

Research Article

Keywords: Hippeastrum hybridum, nanotechnology, AuNPs, biological activities

Posted Date: June 6th, 2022

DOI: https://doi.org/10.21203/rs.3.rs-1639345/v1

Abstract

Nanotechnology is concerned with the production of nanoparticles (NPs) with restricted sizes and shapes through facile, straightforward, and medicinally active phytochemical routes. This study aims to develop an easy and justifiable method for the synthesis of *Hippeastrum hybridum* (HH) induced gold NPs (HH-AuNPs) and then to investigate the effects of these NPs as a free radical scavenger, an inhibitor of the two enzymes i-e Alpha-amylase (α-amylase) and acetylcholinesterase (AChE). UV-Vis spectrum at 576 nm with maximum absorbance at 1.96 confirmed the HH-AuNPs formation. Fourier transform infrared spectroscopy (FT-IR) conforms to the peaks for the functional groups of HH extract and on the surface of HH-AuNPs that are involved in the synthesis and stability of the HH-AuNPs. The average size of 10.72 nm was calculated using four major peaks 38.02°, 44.29°, 64.37°, and 77.58° of X-Rays Diffraction (XRD) analysis. The scanning electron microscope (SEM) analysis confirmed the presence of spherical shaped, monodispersed, and huge density HH-AuNPs with an average size of 30 nm. Energy dispersive X-ray (EDX) confirmed the intense sharp peak at 3.1 keV showing that Au was the main element (48.08%). The HH-AuNPs showed an excellent inhibitory efficacy against free radicals, α-amylase, and AChE as compared to HH extract and $HAuCl_4.3H_2O$ salt. Our results suggest that HH-AuNPs exhibited significant antioxidant, Antidiabetic, and antialzheime activities in a concentration-dependent manner as compared to $HAuCl_4.3H_2O$ and plant extract. However, further investigations are recommended to be able to minimize potential risks of application.

1. Introduction

Nanotechnology is one of the modern techniques of material science which have received much importance in the last many years. It is concerned with the production of nanoparticles (NPs) with restricted sizes and shapes of materials at the nanometer range and is used for the welfare of mankind [1]. Nanoscience is the science in which we have studied phenomena and management of nanomaterials having different properties than those having a larger scale [2, 3]. Application of nanoscience and technology used in applied sciences and as well as material sciences [4]. The importance of NPs science directly depends on the nano size of NPs; because of the sizes, these particles have made their importance in many fields such as medicine, food industries, agricultural wound dressing, chronic ulcers, and oxide fuel batteries for energy storage, cosmetics, and garments [5, 6].

Nowadays, metallic NPs of gold (Au), silver (Ag), copper (Cu), zinc (Zn), titanium (Ti), magnesium (Mg), etc. have been synthesized [7–9]. All Au and Ag have attracted considerable attention in imaging catalysis, sensing, optics, and biomedical devices [10]. NPs can be synthesized in many chemical and physical ways, but these processes generate hazardous byproducts [11]. Green nanotechnology, which uses biological organisms, plant biomass or extracts considered an alternative to the conventional chemical and physical methods in a clean, non-toxic, ecologically sound, and environment-friendly manner [12, 13]. The use of plant materials for the synthesis of NPs could be more advantageous because it does not require elaborate processes as various biomolecules like Ascorbic acids, Citric acid, flavonoids, dehydrogenases, phenols, saponins, and tannins in the plants play a vital role in Ag and Au

reduction [7, 14, 15]. Other compounds that have been used in the formation of AuNPs with antidiabetic properties include chitosan, chondroitin sulfate, tyrosine, and tryptophan [16, 17]. Alpha-amylase, (α-amylase) is an important enzyme in the human body responsible for the metabolism of starch i.e., it converts polysaccharides such as starch and glycogen into disaccharides and oligosaccharides. The inhibition of α-amylase by NPs slows down the carbohydrate digestion and can control the reduction in glucose absorption rate [18].

Like the metal-reducing ability of plant extracts, the antioxidants activity has been associated with the plants' phenolic [19]. [20] argued that antioxidants possess free radical scavenging properties, hence, they play role in promoting health and preventing diseases. Several antioxidant activities [21–24] have been carried out on AuNPs through the green route. Antioxidants extracted from plants play an important role in the prevention of Alzheimer's disease (AD). AD is the most common form of dementia among elderly people that causes problems with memory, thinking, and behavior. Maintaining the levels of acetylcholine (ACh) by inhibition of the acetylcholinesterase enzyme (AChE) is an important strategy to treat AD [25]. AChE inhibitors like tacrine, donepezil, and galantamine are well-known drugs in the treatment of AD which have separated from herbal sources. Although several reports on the screening of AChE inhibitors from herbal sources have been made [26–28], no attention has been given to inhibitor activity of plant-mediated AuNPs so far.

Hippeastrum hybridum (HH) is an ornamental bulbous flowering plant belonging to the family Amaryllidaceae, it has large and showy flowers with many bright colors and is commonly known as Royal Dutch Amaryllis [29]. Normally it produces 2–3 bulblets in a year of growth [30]. HH plant is commonly used in physiological and ecological research, but the extent of their genomic and genetic resources remains limited [31]. Today, a vast majority of plants used in traditional medicine in Pakistan have not been evaluated for their synthesis of AuNPs. The present investigation was, therefore, undertaken to evaluate its AuNPs synthesis, and then evaluated for antioxidant, anti-cholinesterase, and antidiabetic potential.

2. Materials And Methods

2.1. Materials

Hydrogen tetrachloroaurate (III) trihydrate ($HAuCl_4.3H_2O$) obtained from Central Chemical Lahore, was used as the source of AuIII ions. HH plant was collected in September from district Bannu Khyber Pakhtunkhwa and was identified by Dr. Tahir Iqbal, at the Department of Botany, University of Science and Technology Bannu. Potassium ferricyanide, ferric chloride, Trichloroacetic acid, Sulphuric acid, Sodium phosphate, Ammonium molybdenum, ascorbic acid, DPPH (1,1-Diphenyl-2-picrylhydrazyl), H2O2 (Hydrogen peroxide), ABTS (2, 2 azobis, 3-ethyl benzothiazoline-6-sulphonic acid, potassium persulfate ($K_2S_2O_8$), Potato starch, sodium acetate buffer, sodium potassium tartrate, 3, 5 dinitro salicylic acid (DNSA), standard (Glucophage), α-amylase, AChE, ACh, DTNB [5,5´-dithiobis(2-nitro-benzoic acid)], bovine serum albumin, and Coomassie Brilliant blue R-250 were purchased from Sigma (USA). Sodium

dihydrogen phosphate and disodium hydrogen phosphate were purchased from Neon Comercial LTDA (Brazil); and Tris (hydroxymethyl aminomethane) from Vetec (Brazil). All other reagents used were of analytical grade.

2.2. Plant's extraction

After identification the plant was washed using water, shade dried, and ground to a fine powder. About 250 g of the fine plant powder was mixed with 70% methanol in 1:3 and kept on an orbital shaker at 120 rpm for 12 h and then placed at room temperature for 7 days, thus after the 7 days the plant is extracted, and filtered by using Whatman filter paper No 1 and concentrated with the help of the rotary evaporator, after the concentration the extra methanol was evaporated at 37°C to obtain a pure crude methanolic extract of sample and was then reserved in the refrigerator at 4°C for more studies [32].

2.3. Synthesis of HH induced gold nanoparticles (HH-AuNPs)

HH-AuNPs were synthesized from HH plant extract by following the standard protocol [33]. About 10 mM (0.01 M) solution of $HAuCl_4.3H_2O$ was prepared in 50 mL to deionize water. The 10 mM $HAuCl_4.3H_2O$ was further diluted 10 times to obtain a 1 mM $HAuCl_4.3H_2O$ solution. 0.1 M NaOH, ≥ 98%, and 0.1M HCl were used to adjust the pH. An aqueous solution of HH extracts was prepared by dissolving 1 gm of plant extract in 100 mL of deionized water. For dissolution, it is gently stirred on a magnetic stirrer for about 1 hr. After the complete dissolution, it was centrifuged at 6000 rpm for 30 min. The supernatant was collected for activity and the pallets were discarded. The plant supernatant (50 mL) was mixed with the 500 mL of 1 mM $HAuCl_4.3H_2O$ solution of pH 4. The resulting solution changed from golden yellow to crimson red and then finally to ruby red at an optimized ratio after a few hrs at pH 4 and 40ºC temperature. This change in coloration indicated the formation of AuNPs. The solution was then stored for 24 hrs for the complete settlement of NPs and was then monitored using UV–Visible spectrophotometer. The colloidal suspension thus obtained was centrifuged by cold centrifuge at -4°C at 10,000 rpm for 10 min and the pellet was obtained after discarding supermen's. The synthesized NPs were lyophilized to obtain the powder form. The powdered is further characterized and tested for different biological activities.

2.4. Factors affecting synthesis rate, size, and shape of HH-AuNPs

AuNPs synthesis was determined by using different intrinsic factors such as pH, $HAuCl_4.3H_2O$ concentration, HH extract concentration, Temperature, Time, and stability time. To study the effect of basic and acidic conditions pH of the reaction mixture was maintained from 4–12 by using 0.1 M NaOH and 0.1 M HCl solution. To study the effect of HH extract concentration on AuNPs synthesis its concentration varied from 0.5, 1, 1.5, and 2 mL. To study the effect of $HAuCl_4.3H_2O$ salt concentration; its concentration varied to 0.25, 0.5, 1, and 1.5 mM. To study the temperature effect AuNPs synthesis was carried out under different temperature ranges (20, 40, 60, 80, and 100ºC). To study the time of

completion of the reaction AuNPs were synthesized at different time intervals (1 hr, 2 hrs, 3hrs, and 24 hrs). The synthesized AuNPs stability was studied after 1 day, 3 months, and 6 months.

2.5. Characterization of HH-AuNPs

HH-AuNPs concentration in the aqueous solution was definite by using SHIMADZU UV SPECTROPHOTOMETER (UV-1800). The purified HH-AuNPs and HH plants extract was examined for the presence of different phytochemicals by using Fourier Transform-Infrared (FT-IR) Shimadzu (IR Prestige-21) spectrometer (Japan). The crystalline nature of the HH-AuNPs was determined by using the JDX-3532 (JEOL JAPAN) X-ray diffractometer (XRD) with λ-1.54 Aº wavelength. The size and shape of HH-AuNPs were determined by using JEOL Scanning Electron Microscope (SEM) Model JSM-5910 (Japan). The presence of elemental Au in synthesized HH-AuNPs was determined by using electron diffraction X-ray spectroscopy (EDX).

2.6. Biological activities

2.6.1. Antioxidant assays

2.6.1.1. Ferric-Reducing Antioxidant Power screening

The reducing power potential of HAuCl4.3H2O, HH extract, and HH-AuNPs was done by following [34] method with a slight modification. About 2 mL samples (HAuCl4.3H2O, HH extract, and HH-AuNPs), 2 mL of 10 mg/mL potassium ferricyanide, and 2 mL of 0.2 phosphate buffer (pH 6.6) were mixed and followed by incubation for 20 min at 50°C. After incubation 2 mL of 100 mg/mL Trichloroacetic acid was mixed with the solution. About 2 mL of the above solution was mixed with 0.4 mL of 0.1% ferric chloride and 2 mL of deionized H2O followed by incubation for 10 min. Absorbance was observed at 700 nm by spectrophotometer. All samples were run in triplicate. The %age was determined by using the formula (i);

$$\%\ \textbf{Scavenging} = \frac{Ac-As}{Ac} \times 100 \qquad \textbf{(i)}$$

Ac is the control absorbance and As is the sample absorbance

2.6.1.2. Ammonium molybdenum assay

The Ammonium molybdenum antioxidant potential of HAuCl4.3H2O salt, HH, and HH-AuNPs was carried by following [35] procedure. About 1 mL of different concentrations of HAuCl4.3H2O, HH extract, and HH-AuNPs (40–160 µg/mL) and 9 mL of (28 mM sodium phosphate, 600 mM Sulphuric acid, and 4 mM Ammonium molybdenum) were mixed in test tubes. The test tubes were capped with aluminum foil and followed by incubation for 90 min at 95ºC in a water bath. After 90 min of incubation, the mixture was then cool to room temperature and absorbance was noted at 695 nm by spectrophotometer. All samples were run in triplicate. The %age scavenging of Ammonium molybdenum was deliberated by using the formula (i).

2.6.1.3. DPPH activity

1,1-Diphenyl-2-picrylhydrazyl (DPPH) antioxidant potential was carried by following [36] method. Stock solutions (1 mg/mL) of $HAuCl_4.3H_2O$, HH, and HH-AuNPs were prepared in deionized water which was further diluted into (40, 80,100, and 160 µg/mL). Standard ascorbic acid is also prepared in a similar concentration. About 200 µL from different concentrations of $HAuCl_4.3H_2O$, HH, HH-AgNPs, and the standard was mixed with 800 µL of DPPH (1.5 mg/50mL methanol) and then incubated for 30 min in dark a room temperature. Absorbance spectra were recorded at 517 nm by using a UV spectrophotometer against water as a reference. All samples were run in triplicate. The %age scavenging was deliberated by using the equation (i).

2.6.1.4. Hydrogen peroxide scavenging (H_2O_2)

The H_2O_2 scavenging activity was analyzed by [37] method with certain modifications. About 200 µL from various concentrations (40 to160 µg/mL) of $HAuCl_4.3H_2O$, HH, and HH-AuNPs in deionized water, 400 µL of 2 mM H_2O_2, and 400 µL of 50 mM phosphate buffer (pH 7.4) were mixed and followed by the incubation for 20 minutes at 35ºC. The absorbance was recorded by using a spectrophotometer at 610 nm against phosphate buffer as blank. All samples were run in triplicate. The %age was determined by using the equation (i).

2.6.1.5. ABTS screening assay

The ABTS free radical scavenging activity of $HAuCl_4.3H_2O$, HH extract, and HH-AuNPs was accomplished by [38] procedure with slight modification. About 7 mM of ABTS solution and 2.45 mM of potassium persulfate ($K_2S_2O_8$) solution was prepared in deionized water. These two solutions were mixed and allowed for overnight incubation, dark coloration indicated the existence of ABTS•+ free radicals in the solution. The optical density of the mixture was determined using a spectrophotometer and was brought to 0.700 (± 0.02) by the addition of more solvent. About 300 µL of $HAuCl_4.3H_2O$, HH extract, and HH-AuNPs (40 to 160 µg/mL) and standard mixed with 300 µL of ($K_2S_2O_8$ + ABTS) mixture. The absorbance was recorded immediately after mixing the solution at 734 nm by using a spectrophotometer. All samples were run in triplicate. The %age scavenging was deliberated by using the equation (i).

2.6.2. Anti-α-amylase activity

Inhibition of α-amylase activity was determined using 3,5 dinitro salicylic acid (DNSA) [39]. To an obtained starch solution (1% w/v) 1 gram of potato starch was dissolved in 100 mL of 16 mM $C_2H_3NaO_2$ (Sodium acetate) buffer. To obtained enzyme solution 0.5 mg/mL α-amylase from stock (250 units/mL) was dissolved in 1 mL dH_2O. Sodium potassium tartrate and DNSA (96 mM) mixtures were used as a calorimetric reagent. The stock solution of HAuCl4.3H2O, HH extract, HH-AuNPs, and standard (Glucophage) was prepared at 1 mg/mL and was further diluted into different sub-solutions i.e. 25, 50, 75, and 100 µg/mL. Samples were added to 250 µL of α-amylase. The mixture was pre-incubated at 25°C for 10 min and 250 µL of 1% starch prepared in 20 mM sodium phosphate buffer (pH 6.9) was added. The reaction mixtures were incubated at 25°C for 10 min. The reactions were stopped by incubating the mixture in a boiling water bath for 5 min after adding 250 µL from the combined mixture of DNSA and

sodium potassium tartrate. The reaction mixtures were cooled to room temperature, diluted to 1:5 ratios with deionized water, and absorbance was measured in a spectrophotometer (double beam UV-1602, BMS-spectrophotometer) at 450 nm. The Glucophage served as a positive control. All samples were run in triplicate. The percentage of inhibition of enzyme activity was calculated by using the formula (i).

2.6.2.1. Mode of α-amylase inhibition assay

The mode of inhibition of α-amylase is determined as described before [40]. For α-amylase, the enzyme solution (250 units/mL) was pre-incubated with samples (25, 50, 75 and 100 µg/mL). The reactions were started by adding 100, 200, and 300 mg of potato starch and continued at 25°C for 10 min. The reactions were stopped by adding 0.25 mL of DNSA followed by boiling for 5 min. The reaction mixtures were cooled to room temperature, diluted to a 1:5 ratio with dH_2O, and absorbance was measured in a spectrophotometer (double beam UV-1602, BMS-spectrophotometer) at a 450 nm Double reciprocal plot (1/V versus 1/[S]) where V is reaction velocity and [S] is substrate concentration was plotted. The mode of inhibition was determined by analyzing the Lineweaver-Burk plot using Michaelis-Menten kinetics [41]. Michaelis constants *(K_m)* were determined by two different plots of 1/V vs. 1/S [41] and V vs. V/S [42, 43]. The K_i and *KI* values were obtained using the Cornish-Bowden plot of S/V vs. [I] and Dixon plot 1/V vs. [I] [44, 45] respectively. IC_{50} was determined by percentage residual activity and percentage inhibition versus concentration of HH extract and HH-AuNPs.

2.6.3. Anti-cholinesterase activity

2.6.3.1. Venom

Venom from live *Bungarus sindanus* snakes was squeezed out manually, lyophilized immediately, and stored at − 20°C for further use. The study was approved by the Departmental Ethical Approval Committee, ref. n. Biotech/Ethic/110.

2.6.3.2. Anti-cholinesterase assay

AChE activity was determined by the method of [46] modified by [47] using a double beam spectrophotometer UV-1602, BMS biotechnology medical service. Hydrolysis rates (V) were measured at various acetylthiocholine (S) concentrations (0.05–1 mM) in a 1 mL assay mixture with 50 mM phosphate buffer, pH 7.4, and 10 mM DTNB at 25oC. About 20 µL of diluted snake venom was also added and the reaction mixture was incubated for 5 minutes at 37^oC. The enzyme-substrate reaction immediately started upon the addition of different concentrations of substrate. The hydrolysis was scrutinized by the formation of thiolate di-anion of DTNB every 15 seconds for 90 seconds using a spectrophotometer. The amount of the yellow color develops is a measure of the activity of AChE. All samples were run in triplicate.

2.6.3.3. Protein determination

The protein content of the enzyme preparation was assayed by the method of Bradford [48] using bovine serum albumin as a standard.

2.6.3.4. Kinetic determinations

The interaction of HH extract/HH-AuNPs, and AChE was determined using the [41] double reciprocal plot, by plotting 1/V against 1/[S] analyzed over a range of ACh concentrations (0.05–1 mM) in the absence and presence of extract (10, 20, and 30 µg/mL). A double reciprocal plot (1/V versus 1/[S]) where V is reaction velocity and [S] is substrate concentration was plotted. The mode of inhibition was determined by analyzing the Lineweaver-Burk plot using Michaelis-Menten kinetics [41]. Michaelis constants *(Km*) were determined by two different plots of 1/V vs. 1/S [41] and V vs. V/S [42, 43]. The *Ki* and *KI* values were obtained using the Cornish-Bowden plot of S/V vs. [I] and Dixon plot 1/V vs. [I] [44, 45] respectively. IC50 was determined by percentage residual activity and percentage inhibition versus concentration of HH extract and HH-AuNPs.

2.7. Statistical Analysis

Data were expressed as mean ± standard error of the mean (SEM). Statistical analysis was performed using one-way ANOVA, which was followed by post-hoc analysis (Duncan multiple range test) [49]. The coefficient of correlation was determined by using Statistics (version 8.1 USA). The difference was considered to be significant for $P < 0.05$

3. Results

3.1. Synthesis of HH-AuNPs

3.1.1. UV-visible spectrophotometric analysis of HH-AuNPs

The aqueous AuNPs exhibited ruby red color due to the SPR. After mixing the HH aqueous extract with $HAuCl_4.3H_2O$ the color of the solution start to change from golden yellow to crimson red and then finally to ruby red indicating the bioreduction of the Au + by HH extract. The scale of the length of the spectrophotometer ranged from 200 to 800 nm. Figure 1 indicated 576 nm, absorption bands of the HH-AuNPs, at higher absorption of 1.96 after 24 hrs of incubation at 40ºC.

3.1.2. Factors affecting the synthesis of AuNPs

In the present study; the synthesis of HH-AuNPs was studied under different factors. According to a pH study, HH-AuNPs were synthesized at different basic and acidic conditions (pH 4 to 12). No sharp band was observed in the range of 500–600 nm at higher pH of 8 to 12. The bands become sharp and sharp with decreasing the pH and a final sharp peak of 576 nm with a maximum absorbance of 1.96 was reported at pH 4. See Fig. 2a. According to the HH extract concentration studies different peaks i-e 556, 576, 548, and 550 were observed with a maximum absorbance of 0.6893, 1.96, 1.9135, and 1.7776 at the volume of 0.5, 1, 1.5, and 2 mL respectively. See Fig. 2b. The UV-vis spectra of HH-AuNPs aqueous

medium at different HAuCl4.3H2O concentrations (0.25–1.5 mM) were noted in the range of 200 to 800 nm wavelength which indicated broader bands at 0.25, 0.5, and 1.5 mM with low absorbance but a sharp peak 576 nm with maximum absorbance 1.96 was obtained at 1 mM (See Fig. 2c). HH-AuNPs synthesis was studied by incubating the reaction mixture at different temperature ranges (20 to 100ºC). A sharp band at 576 nm was obtained at 40ºC with a maximum absorbance of 1.96, but with an increase in temperature beyond 40ºC the band becomes broad and broader i-e 558, 546, and 567 nm with a maximum absorbance of 1.0505 0.9098, and 0.7089 were reported at 60, 80, and 100ºC respectively. See Fig. 2d. Figure 2e indicated the effect of reaction time on the synthesis of HH reduced AuNPs. Broad peaks with lower absorption appeared after 1hr, 2hrs, and 3hrs of the stirring (685, 654, and 500 nm with a maximum absorbance of 0.251, 0.182, and 0.54 respectively). Due to the continuous reduction of Au ions by HH extract the absorption peak increases over time. A final clear sharp peak of 576 nm at high absorbance 1.96 was observed after 24 hrs of the HH and Au ions reaction. The stability of the HH reduced AuNPs was studied at different periods (1 day, 3 months, and 6 months). A sharp peak of 576 nm with a maximum absorbance of 1.96 appeared after 1 day of AuNPs formation; but after 3 and 6 months this peak become broad i-e 558 nm after 3 months and 567 nm after 6 months, with low absorbance of 1.0505 and 0.7089 respectively. (See Fig. 2f).

3.2. FT-IR analysis of HE extract and HH-AuNPs

The FTIR spectrum of HH extracts and HH-AuNPs (prepared in water) is given in Fig. 3. The data on the peak values and the probable functional groups (obtained by FTIR analysis) present in the HH extract and HH-AuNPs are presented in Table 1. The characteristic absorption band were exhibited in the range 3400-3200cm^{-1} (for O-H stretch), 2935–2915cm^{-1} (for –CH (CH_2) vibration), 2865-2845cm^{-1} (for –CH (CH_2), 2260-2100cm^{-1} (for C ≡ C stretch), 2100-1800cm^{-1} (for C = O frequency), 1740-1725cm^{-1} (for C = O stretch), 1650-1600cm^{-1} (for C = O stretch), 1410-1310cm^{-1} (for O-H bend), 1340-1250cm^{-1} (for CN stretch), 1100-1000cm^{-1} (for Phosphate ion), 995-850cm^{-1} (for P-O-C stretch), 800-700cm^{-1} (for C-Cl stretch), 700-600cm^{-1}(for C-Br stretch), and 690-550cm^{-1} (for C-Br stretch) were exhibited by HH extract and HH-AuNPs.

Table 1
FTIR Interpretation of compounds in HH whole plant extract and HH-AuNPs

S. No	Wave number cm^{-1} [Reference article]	Wave number cm^{-1} [HH-plant]	Wave number cm^{-1} [HH-AuNPs	Functional group assignment	Phyto compounds Identified
1	3400 – 3200	3266.48	3324.90	O-H stretch	Poly Hydroxy compound
2	2935–2915	2917.21	2922.72	Asymmetric stretching of –CH (CH_2) vibration	Saturated aliphatic compound-Lipids
3	2865 – 2845	2855.98	2852.04	Symmetric stretching of –CH (CH_2) vibration,	Lipids, protein
4	2260 – 2100	2259.95	2245.12	Carbon-Carbon triple bond	Terminal alkynes
5	2100 – 1800	1985.34	1963.9	Carbonyl compound frequency	Transition metal carbonyls
6	1740 – 1725	1740.10	1729	C = O stretch	Aldehyde compound
7	1650 – 1600	1608.02	1638.20	C = O stretching vibration, Ketone group	Ketone compound
8	1410 – 1310	1410	1410	O-H bend, Alcoholic group	Phenol or tertiary alcohol
9	1340 – 1250	1290.95	1250	CN stretch	Aromatic primary amine
10	1100 – 1000	1035.52	1010.16	Phosphate ion	Phosphate compound
11	995 – 850	852.68	852.1	P-O-C stretch	Aromatic phosphates
12	800 – 700	743.11	714.42	C-Cl stretch	Aliphatic Chloro compound
13	700 – 600	676.003	622.61	C-Br stretch	Aliphatic bromo compounds
14	690 – 550	571.91	555.2	Halogen compounds (Bromo-compounds)	Aliphatic Bromo compounds

3.3. XRD analysis of HH-AuNPs

XRD is a technique that is used for determining the size and crystalline nature of the sample. In the present study, the HH-AuNPs were analyzed by XRD. Figure 4 indicated 4 Bragg reflections at angles of

38.02°, 44.29°, 64.37°, and 77.58° which are corresponded to the planes (1 1 1), (2 0 0), (2 2 0), and (3 1 1) respectively. These reflections can be indexed conferring to the face of the face-centered cubic crystal structure of Au ion. The “d’ (interplanar spacing) and “a” (Miller constants) values were calculated by using the Debye-Sherrer’s equation (i) and (ii) respectively;

$$dhkl = \pi/2\sin\theta hkl \quad \text{(i)}$$

$$a^{o} = dhkl(h2 + k2 + l2)1/2 \quad \text{(ii)}$$

Results are tabulated in Table 2.

Table 2
Determination of Interplaner spacing and lattice constant of HH-AuNPs

S. no	2θ Value	Element	plane	Interplaner spacing (d)	Lattice constants (a_0)
1	38.02	Au	1 1 1	2.36 Å	4.08 Å
2	44.29	Au	2 0 0	2.06 Å	4.08 Å
3	64.37	Au	2 2 0	1.44 Å	4.07 Å
4	77.58	Au	3 1 1	1.22 Å	4.04 Å

Table 3
The HH and HH-AuNPs concentrations providing 50% inhibition (IC_{50}) values of the different antioxidants activities.

IC_{50} (µg/mL)			
Assays	**Ascorbic Acid**	**HH extract**	**HH AuNPs**
Ferric reducing	79 ± 0.06	151 ± 0.13	95.17 ± 0.025
Molybdenum scavenging	48 ± 0.11	91.48 ± 0.13	58.5 ± 0.051
DPPH scavenging	52.38 ± 0.21	156 ± 0.31	136.17 ± 0.071
H_2O_2 scavenging	51.18 ± 0.3	136 ± 0.21	105.66 ± 0.062
ABTS scavenging	40.059 ± 0.0.05	154.12 ± 0.03	144.82 ± 0.072

Table 4
Effect of Glucophage, HH extract and HH-AuNPs on K_m and V_{max} of α-amylase.

HH AuNPs			
Concentrations (µg)	**K_m (mg)**	**V_{max}(µmol α-amylase/min/mg protein)**	**%Decrease**
0	**66.171**	**0.0265**	**0**
25	**66.63**	**0.023**	**13.20**
50	**67.03**	**0.0225**	**15.094**
75	**66.77**	**0.0215**	**18.96**
100	**66.85**	**0.0184**	**30.56**

A

HH extract			
Concentrations (µg)	K_m (mg)	%Increase	V_{max}(µmol α-amylase/min/mg protein)
0	68.50	0	0.0269
25	75.8	10.65	0.0264
50	91.4	33.43	0.0264
75	111.64	62.9	0.0271
100	126.33	84.37	0.0267

B

Glucophage

Concentrations (µg)	K_m (mg)	%Decrease	V_{max}(µmol α-amylase/min/mg protein)	%Decrease
0	194.56	0	0.0566	0
25	115.78	40.49	0.0346	38.86
50	80.49	58.74	0.0252	55.47
75	67.78	56.6	0.0216	61.83
100	60.012	69.15	0.0172	69.61

C

Table 5

Effect of HH extract, HH AuNPs, and Glucophage on K_{lapp} and $V_{maxiapp}$ of α-amylase. The $V_{maxiapp}$ and K_{lapp} were determined from Dixon plot of 7A and 7B for α-amylase. The $V_{maxiapp}$ is equal to the reciprocal of y-axis intersection of each line for each potato starch concentration while K_{lapp} is equal to the x-axis intersection in Dixon plot.

HH-AuNPs			
[Potato starch] (mg)	**K_{lapp} (µg)**	**$V_{maxiapp}$ (µg / min / mg)**	**% Decrease**
100	**261.74**	**0.016**	**0**
200	**260.22**	**0.018**	**12.5**
300	**263.78**	**0.022**	**37.5**

A

HH Extract			
[Potato starch] (mg)	K_{lapp} (µg)	% Increase	$V_{maxiapp}$ (µg / min / mg)
100	139.53	0	0.20
200	317.64	127.64	0.20
300	634	354.33	0.22

B

Glucophage			
K_{lapp} (µg)	% Decrease	$V_{maxiapp}$ (µg / min / mg)	% Increase
128.30	0	0.0198	0
106.95	16.64	0.025	26.26
69.44	46	0.037	89

C

Table 6
Comparative study of kinetic parameters of α-amylase inhibition by HH extract, HH-AuNPs, and Glucophage; K_i, inhibition constant; K_I, dissociation constant of the α-amylase–Pottao starch–HH complex into the α-amylase–Pottao starch complex and free HH; K_m, Michaelis–Menten constant and $IC_{50,}$ 50% inhibitory concentration.

Parameters	HH AuNPs	HH Extract	Glucophage
K_i (µg)	25	26	12
K_I (µg)	261.91	364	101.56
K_m (mg)	66	68.06	195
IC_{50} (µg)	44.33 ± 0.042	56 ± 0.003	37 ± 0.13

Table 7
Influence of HH and HH-AuNPs on K_m and V_{max} of *Bungarus Sindanus* (Krait) venom AChE.

S.no	HH-AuNPs				HH extract		
Concentrations (µg)	K_m (mM)	% Decrease	V_{max} (µmol / min per mg protein)	% Decrease	K_m (mM)	V_{max} (µmol / min per mg protein)	% Decrease
0	0.197	0	56.94	0	0.049	157.33	0
10	0.1025	47.96	29.98	47.34	0.049	62.85	60.05
20	0.059	70.05	19.79	65.24	0.053	48.47	69.19
30	0.050	74.61	15.93	72.02	0.049	40.89	74.01

Table 8

Effect of HH extract and HH-AuNPs on K_{lapp} and $V_{maxiapp}$ of *Bungarus Sindanus* (Krait) venom AChE. The $V_{maxiapp}$ and K_{lapp} were determined from Dixon plot of Fig. 12 for snake venom, AChE. The $V_{maxiapp}$ is equal to the reciprocal of y-axis intersection of each line for each AcSCh concentration while K_{lapp} is equal to the x-axis intersection in Dixon plot.

S.no	HH-AuNPs				HH extract		
[ASCh] (mM)	K_{lapp} (mM)	%Decrease	$V_{maxiapp}$ (µmol / min per mg protein)	%Decrease	K_{lapp} (mM)	$V_{maxiapp}$ (µmol / min per mg protein)	% Decrease
0.05	80.75	0	11.62	0	36.49	38.29	0
0.1	55.02	32	16.08	38.38	36	57.38	49.85
0.25	39.123	51.55	22.34	92.25	36.13	60	56.6
0.5	28.46	64.75	33.78	190.70	36.24	68.46	78.79
1	23.81	70.51	41.73	259.122	36.47	77.23	104.42

Table 9

Study of kinetic parameters of AChE inhibition by HH-AuNPs and HH extract. K_i, inhibition constant; K_I, dissociation constant of the AChE–ASCh–HH complex into the AChE–ASCh/BSCh complex and free HH; K_m, Michaelis–Menten constant, and $IC_{50,}$ 50% inhibitory concentration.

Parameters	HH-AuNPs	HH extract
K_i (µg)	23	32
K_I (µg)	45.43	36.25
K_m (mM)	0.195	0.052
IC_{50} (µg)	16.66 ± 0.011	19.1 ± 0.021

The average crystalline size of HH induced AuNPs is calculated by using the Debye-Sherrer's formula (iii);

$$D = k\lambda/\beta\cos\theta \qquad \text{(iii)}$$

D is the average crystalline size, k is a geometric factor (0.9), λ is the wavelength of the X-ray radiation source and β is the angular FWHM (full-width at half maximum) of the XRD peak at the diffraction angle θ. For the four major peaks i-e 38.02°, 44.29°, 64.37°, and 77.58° the average calculated crystalline size was found to be 10.72 nm.

3.4. SEM analysis of HH-AuNPs

In the present study; HH-AuNPs were screened by SEM to determine their surface morphology. SEM results showed that the HH-AuNPs are monodispersed, spherical-shaped, and are in high density (Fig. 5). The average particle size was calculated using Nano measurer software by marking 15 particles and was found to be 30 nm (0.03 µm).

3.5. EDX analysis of HH-AuNPs

The elemental constituents and relative abundance of the biosynthesized AuNPs were obtained from EDX analysis as shown in Fig. 6. EDX spectrometers confirmed the presence of elemental Au signal of the AuNPs with 48.08%. The vertical axis displays the number of X-ray counts while the horizontal axis displays energy in KeV. Identification lines for the major emission energies for Au are displayed and these correspond with peaks in the spectrum, thus giving confidence that Au has been correctly identified in HH-AuNPs. Thus the EDX spectrum discloses the purity and the complete chemical composition of HH-AuNPs. The other elements served as capping organic agents bound to the surface of the HH-AuNPs.

3.6. Antioxidant assays

3.6.1. Ferric reducing power assay (FRPA)

In the present study; different concentrations (40, 80, 120, and 160µg/mL) of $HAuCl_4.3H_2O$ salt, HH extract, HH-AuNPs, and ascorbic acid were tested for ferric reducing activity. The obtained results indicated that all the tested samples showed ferric reducing potential in a dose-dependent manner and showed maximum scavenging of 16.92 ± 0.014 ($HAuCl_4.3H_2O$), 55.2 ± 0.035% (HH extract), and 77.2 ± 0.014 (HH-AuNPs); while the positive control ascorbic acid showed 84.4 ± 0.016% scavenging at the highest 160 µg/mL concentration (Fig. 7a). All the samples i-e HH extract, HH-AuNPs, and Ascorbic acid cause 50% scavenging (IC_{50}) at 151 ± 0.13, 95.17 ± 0.025, and 79 ± 0.06 µg/mL respectively; while the $HAuCl_4.3H_2O$ does not cause 50% inhibition. (See the Table. 3).

3.6.2. Ammonium molybdenum assay

Different concentrations (40–160 µg/mL) of $HAuCl_4.3H_2O$ salt, HH extract, HH-AuNPs, and ascorbic acid were tested for their Ammonium molybdenum scavenging assay (See Fig. 7b). $HAuCl_4.3H_2O$ salt, HH extracts, HH-AuNPs, and ascorbic acid showed maximum scavenging potential of 22 ± 0.0014, 62.1 ± 0.0021, 74.3 ± 0.021, and 88.8 ± 0.001% at 160 µg/mL. The calculated IC_{50} values were found to be 91.48 ± 0.13 for HH extract, 58.5 ± 0.051 for HH-AuNPs, and 48 ± 0.11 µg/mL for ascorbic acid respectively; while the $HAuCl_4.3H_2O$ does not cause 50% scavenging of Ammonium molybdenum (See the Table. 3).

3.6.3. DDPH scavenging assay

Different concentrations of $HAuCl_4.3H_2O$ salt, HH extract, HH-AuNPs, and ascorbic acid (40, 80, 120, and 160µg/mL) were tested for their DPPH scavenging activity. The obtained results indicated that

$HAuCl_4.3H_2O$ salt, HH extract, HH-AuNPs, and ascorbic acid showed DPPH scavenging potential in a dose-dependent manner and showed maximum scavenging of 21 ± 0.007, 55 ± 0.059, 58.6 ± 0.51, and 90 ± 0.0014% % at 160µg/mL respectively (Fig. 7c). All the samples except $HAuCl_4.3H_2O$ salt showed 50% DPPH scavenging activity. The calculated IC_{50} (50% inhibition) values were found to be 156 ± 0.31for HH extract, 136.17 ± 0.071 for HH-AuNPs, and 52.38 ± 0.03 µg/mL for Ascorbic acid respectively. Results are tabulated in Table. 3.

3.6.4. Hydrogen peroxide scavenging (H_2O_2)

In the current research work; different concentrations (40–160 µg/mL) of $HAuCl_4.3H_2O$ salt, HH extract, HH-AuNPs, and ascorbic acid were tested for their H_2O_2 scavenging activity (Fig. 7d). $HAuCl_4.3H_2O$ salt, HH extract, HH-AuNPs, and ascorbic acid showed maximum scavenging potential of 21 ± 0.021, 56.6 ± 0.0021, 62 ± 0.041, and 76.6 ± 0.0014% at 160 µg/mL with IC_{50} values of 136 ± 0.21 for HH extract, 105.66 ± 0.062 for HH-AuNPs, and 51.18 ± 0.3 µg/mL for ascorbic acid respectively; while the $HAuCl_4.3H_2O$ does not cause 50% inhibition of H_2O_2. (See the Table. 3).

3.6.5. ABTS screening assay

The present study indicated the ABTS scavenging potential of $HAuCl_4.3H_2O$ salt, HH extract, HH-AuNPs, and ascorbic acid at various concentrations (40–160 µg/mL). Figure 7e indicated that $HAuCl_4.3H_2O$ salt, HH extract, HH-AuNPs, and ascorbic acid scavenge ABTS free radicals in dose-dependent manner and indicated 21 ± 0.0014, 55.1 ± 0.004, 59 ± 0.05, and 90 ± 0.002% inhibition at the highest concentration (160 µg/mL) with an IC_{50} of 154.12 ± 0.03 for HH extract, 144.82 ± 0.072 for HH-AuNPs, and 40.059 ± 0.0.05µg/mL for ascorbic acid respectively; while $HAuCl_4.3H_2O$ salt does not show 50% scavenging of ABTS free radicals. (See the Table. 3).

3.7. Antidiabetic activity

3.7.1. Anti-α-amylase activity

The $HAuCl_4.3H_2O$ salt, extracts of HH, HH-AuNPs, and standard drug Glucophage were tested to evaluate theirs in vitro inhibition abilities against α-amylase. All the samples inhibit α-amylase in dose-dependent manner (25, 50, 75, and 100 µg/mL) and cause maximum inhibition of 7 ± 0.0014% ($HAuCl_4.3H_2O$ salt), 66 ± 0.003% (HH extract), 71 ± 0.032% (HH-AuNPs), and 85 ± 0.0014% (Glucophage) respectively at fixed (1%) substrate concentration (Fig. 8).

3.7.2. Effects of HH, HH-AuNPs, and Glucophage on K_m and V_{max}

The effect of HH, HH-AuNPs and Glucophage on K_m and V_{max} of α-amylase were calculated. Statistical analysis indicated that HH-AuNPs cause a non-competitive type of inhibition K_m to remain constant and V_{max} decrease from 13.20 to 30.56% (Fig. 9a), similarly HH causes a competitive type of inhibition of α-

amylase i-e. K_m increases from 10.65 to 84.37%, while V_{max} remained constant (Fig. 9b), while in the case of Glucophage uncompetitive type of inhibition was observed i-e. Both K_m and V_{max} decreased from 40.49 to 69.15 and 38.86 to 69.61% respectively (Fig. 9c). Results are presented in Table. 4A, 4B, and 4C.

3.7.3. Effects of HH, HH-AuNPs, and Glucophage on K_{lapp} and $V_{maxiapp}$

In α-amylase, K_{lapp} remained constant while V_{maxiap} was decreased from 12.5 to 37.5% for HH-AuNPs, while for HH extract the K_{lapp} was found to increase from 127.64 to 354.33% while $V_{maxiapp}$ remained constant with the increase of substrate concentration (100–300 mg). In the case of Glucophage, the K_{lapp} was found to decrease from 16.64 to 46% while $V_{maxiapp}$ decreased from 26.26-to 89% (Table. Table. 5a, 5b, and 5c). The values were calculated from Fig. 10a, 10b, and 10c respectively.

3.7.4. Determination of K_m

K_m values for the hydrolysis of the substrate (potato starch) by α-amylase, were calculated by using the Lineweaver-Burk plot and were found to be 66, 68.06, and 195 mg for HH-AuNPs, HH, and Glucophage respectively. The values are presented in Table. 6.

3.7.5. Determination of K_I and K_i

K_I (constant of α-amylase–Potato starch–HH-AuNPs, HH extract/Glucophage complex into α-amylase–Potato starch complex and HH-AuNPs, HH extract/Glucophage) was estimated to be 261.91 (Fig. 10a), 364 µg (Fig. 10b), and 101.56 µg (Fig. 10c) for α-amylase respectively, while *Ki* (inhibitory constant) was estimated to be 25, (Fig. 11a), 26 (Fig. 11b) and 12 µg (Fig. 11c) for HH-AuNPs, HH extract, and Glucophage respectively. The values are tabulated in Table. 6.

3.7.6. Determination of IC_{50}

HH-AuNPs, HH extract, and Glucophage cause 50% inhibition (IC_{50}) against α-amylase at a concentration of 44.33 ± 0.042, 56 ± 0.003, and 37 ± 0.13 µg/mL, respectively. The values are tabulated in Table. 6.

3.8. Anti-acetylcholinesterase activity

At fixed substrate acetylthiocholine (ACh) concentration (0.5 mM) $HAuCl_4.3H_2O$ salt, HH plant, and HH-AuNPs exerted 23 ± 0.057, 59 ± 0.003, and 61 ± 0.314% inhibition against the snake krait venom AChE at maximum 30 µg/mL concentration in 1 mL assay mixture (Fig. 12a).

3.8.1. Determination of IC_{50}

The concentration of HH extract and HH-AuNPs that cause 50% inhibition (IC_{50}) of AChE enzyme activity were found to be 19.1 ± 0.021 and 16.66 ± 0.011 µg/mL respectively; while no any concentration of $HAuCl_4.3H_2O$ salt cause 50% inhibition of AChE (Fig. 12b).

3.8.2. Effects of HH on K_m and V_{max}

The effect of HH and HH-AuNPs on K_m and V_{max} of AChE were calculated. HH caused a non-competitive type of inhibition the K_m values remained constant and V_{max} decreased from 60.05–74.01%, while HH-AuNPs caused an uncompetitive type of inhibition in both K_m and V_{max} decreased from 47.96–74.61 and 47.34–72.02% respectively (Fig. 13a and 13b). Values are presented in (Table. 7).

3.8.3. Effects of HH on K_{lapp} and $V_{maxiapp}$

In snake venom AChE, K_{lapp} was found to remain constant, while $V_{maxiapp}$ decreased from 49.85 to 104.42% HH extract, while in the case of HH-AuNPs K_{lapp} decreased from 32-70.51% and $V_{maxiapp}$ decreased from 38.38-259.122% with an increase of substrate (0.05–1 mM) (Table. 8). The values were calculated from Fig. 14a and 14b.

3.8.4. Determination of K_m

K_m values for the hydrolysis of substrate by AChE were calculated by using a Lineweaver-Burk plot and were found to be 0.195 and 0.052 mM for HH-AuNPs and HH extract, respectively. The values are presented in Table. 9.

3.8.5. Determination of K_I and K_i

K_I (constant of AChE–AcSC–HH-AuNPs/HH extract complex into AChE–AcSC complex and HH-AuNPs/HH) was estimated to be 44.43 and 36.25 µg (Fig. 14a and 14b) for AChE, while K_i (inhibitory constant) was estimated to be 23 and 32 µg for HH-AuNPs and HH extract respectively, (Fig. 15a and 15b). The values are presented in Table. 9.

4. Discussion

The synthesis and characterization of NPs and their applications represent a rapidly growing concept and an emerging trend in science and technology [50]. The use of plant materials for the synthesis of NPs could be more advantageous because it does not require elaborate processes [51]. The UV–vis spectroscopy technique can be used to determine the synthesis and stability of AuNPs in an aqueous solution due to their characteristic absorption in the range of 500–600 nm [52, 53]. AuNPs exhibited ruby red color in the aqueous solution due to the excitation of surface plasmon vibrations in the metal NPs which give rise to the surface plasmon resonance (SPR) band [54, 55]. The plasmon resonance (PR) can be pictured as a “wave” of electrons sloshing over the surface of a metal NPs. As a result, an enhanced electromagnetic field at and near the metal NPs surface is set up. The position of the plasmon band (extinction spectrum) is best measured on a conventional UV–vis spectrophotometer and appears as a band with extremely high extinction coefficients [56]. In the present study, when 1 mL of HH aqueous extract was added to 1 mM $HAuCl_4.3H_2O$ solution at pH 4 the color of the solution start to change from golden yellow to crimson red and then finally to ruby red at an optimized ratio after 24 hrs of incubation

at 40ºC. The appearance of the ruddiness color in an aqueous medium is considered the first indication of colloidal AuNPs formation [53, 54]. This color change is due to the reduction of the Au^{+} into HH-AuNPs by the active molecules of the HH aqueous extract such as phenolic, alkaloids, saponins, amino acids, proteins, etc. The absorption spectrum of the aqueous solution revealed a peak at 576 nm with a maximum absorbance of 1.96 after 24 hrs.

Synthesis of the AuNPs is affected by different factors such as plant extract volume, $HAuCl_4.3H_2O$, pH, temperature, time, etc. [57]. An ideal pH is required for synthesis of controlling the shape and size of NPs [58, 59]. The role of pH is significant in changing the size and shape of NPs. Numbers of studies have shown the stability of AuNPs at acidic pH while many achieved stable suspension in the basic region. Furthermore, the synthesis reaction, size, shape, and stability of AuNPs could be controlled by adjusting the initial pH value of the reaction mixture. In the present study, the reaction was performed at different pH ranges from 4 to 12 to identify the effect of pH on the formation of HH-reduced AuNPs. It was detected that the absorbance of the solution increased while changing the initial pH of the solution. With the increase in pH, the SPR band was also blue-shifted to 576 nm at pH 4. The AuNPs were quite stable in an acidic medium; however, a gradual decrease in UV–vis peak intensities showed less stability with an increase in pH of the colloidal solution from 4 to 12. Peak broadening and redshift were noted at pH 10 and 11. UV-vis results suggested that no reaction occurred in the basic region which is in agreement with the previous studies [54]. It was might be due to the deprotonation of hydroxyl and carboxyl groups present in extracts [60]. AuNPs synthesized using banana peel extract were stable at a pH value of 2–5 supporting the results of the present study [61]. A broader range of pH i.e. 2–11 were taken to synthesize AuNPs using oil palm mill effluent and pH 3 was observed optimum to achieve definite shapes particles [62]. Medicinal plants are a rich source of secondary metabolites that act as reducing, capping, and stabilizing agents for NPs. However, the composition of these active secondary metabolites varies from plant to plant depending on the nature, part, type of plant, and method followed for the extraction of these metabolites [63]. In the present study, the SPR peak is blue-shifted from 553 to 576 nm as the added volume of HH extract increased from 0.5 to 1mL; the blue shift of SPR peaks is a sign of the production of small size NPs. The shift towards shorter wavelengths with decreasing NPs size is associated with frequencies of oscillation of different free electrons in the conduction band [64]. The SPR band absorbance increased with an increasing volume of HH extract, which reveal the higher production of AuNPs. This is due to the availability of more reducing agents for the Au ions bioreduction [65]. But the further increase in the volume of HH extract from 1.5 to 2 mL the redshift of SPR was recorded, this redshift is a sign of large size NPs. HH contains active molecules such as carbohydrates, flavones, terpenoids, alkaloids, and proteins that were testified to be responsible for the bio-reduction of Au + to Au^{o}. Proteins and terpenoids are believed to play an important role in AuNPs biosynthesis through the reduction of Au ions, and carbohydrates provide a coating of AuNPs [66, 67]. The HH extract produces more AuNPs than other plant extracts credited to the availability of the larger amount of reducing agents in the extract, such as flavonoid and its antioxidant activity [67]. Varying concentrations of $HAuCl_4.3H_2O$ (0.25 to 1.5 mM) were prepared while the other factors were kept constant i-e HH extract (1 mL), pH (4), temperature (40ºC), and time (24 hrs). At 0.25 and 0.5 mM concentrations of $HAuCl_4.3H_2O$ broad peaks

were revealed; while at increased $HAuCl_4.3H_2O$ concentration (1 mM) a sharp peak of 576 nm with maximum absorbance 1.96 was reported but beyond this concentration the peak becomes broad. Thus it can be reported from the present results that the absorption peak intensity increase with an increase in $HAuCl_4.3H_2O$ salt concentration. All the results of the present study are in good covenant with the results reported in the literature [68]. Temperature is another factor that plays a crucial role in tuning the size and shape of AuNPs. The effect of temperature on the SPR feature of metal NPs is a critical factor in the pure and applied science of the NPs [69, 70]. In the present work, the effect of temperature on AuNPs synthesis was studied at five different temperatures, that is, 20°C, 40°C, 60°C, 80°C, and 100°C, and the UV-vis spectra were recorded after 24 hrs. From the results, it is clear that the rate of AuNPs increase with increasing temperature. Earlier, similar findings related to the increase in the reaction rate of AuNPs synthesis with an increase in reaction temperature have also been reported by [71, 72]. According to the UV-vis spectra of AuNPs synthesized at different temperatures, it is reported that there is a blue shift to 576 nm with a maximum absorbance of 1.96 at 40°C in comparison to the AuNPs synthesized at 20°C. The results suggest that the higher temperature leads to an increase in the activation energy of the molecules and a faster rate of reaction. As a result, there is a decrease in the size of synthesized AuNPs and, hence, monodispersed small NPs are formed without undergoing the phase of particle size growth [73]. However, the present study shows that a further increase in reaction temperature (60°C to 100°C) and an increase in the size of AuNPs were reported as is evident from the sharp and narrow SPR peaks with increased sphericity. These results are consistent with the previous findings discussing the same in context to the increased reaction rate of AuNPs synthesis upon increasing the reaction temperature. The high reaction temperature leads to a rapid nucleation process of metallic NPs involving the enhanced consumption of most of the metal ions with the least secondary reduction of the preformed nuclei [73, 74]. It has been shown that an optimum temperature could help control the rate of AuNPs synthesis and the uniform NPs can be synthesized under optimum pH at different reaction temperatures [75].

The possible role of Phyto-components present in aqueous plant extract responsible for mediating and stabilizing the nanoparticles was depicted using FTIR analysis. A perusal of scientific studies reports FTIR as one of the ideal tools to predict functional moieties. In the present investigation, vibrational stretch occurring at different peaks which corresponds to polyhydroxy, phenol, carboxyl, proteins, lipids, amide, alkynes, alkene etc. Scientific studies on FTIR analysis of plant-mediated NPs report that different functional moieties like hydroxyl, carboxyl, and amide are responsible for the reduction of metal ions to produce NPs [76, 77]. The obtained result of FTIR analysis is by previous findings [78]. Interestingly, in the plant-mediated synthesis of NPs, the Phyto-components also play important role in the stabilization of NPs which is very crucial for rendering its applicative properties. These results also coincide with reports of earlier findings [79, 80].

XRD is used for the phase identification and characterization of the crystal structure of the AuNPs. XRD analysis of HH-AuNPs shows four distinct peaks at 38.02°, 44.29°, 64.37°, and 77.58° which are corresponded to the planes (1 1 1), (2 0 0), (2 2 0), and (3 1 1) respectively. The mean size for HH-AuNPs was calculated using Debye-Sherrer's equation is 10.72 nm. The "d" and "a" values were calculated by

using Debye-Sherrer's equation. To fulfill Bragg's Law the incidence theta (θ) must vary with the change in "d" values which showed that as the value of θ increases the "d" values of the atomic layers decrease. Similar results were also reported by [7, 81].

SEM was used to confirm the production and examine the morphology characterization at the nm to μm scale of the obtained AuNPs [82]. In the present study, the SEM data revealed that the AuNPs were spherical with an average particle size of 30 nm. SEM analysis shows uniformly distributed HH-AuNPs that indicate the stabilization of AuNPs by HH extract capping agents. Green synthesis of spherical shape AuNPs with particle size range from 21 to 45 nm was carried out by using *Stevia rebadiauna* leaf extracts are in good accordance with the results of the present research work [81].

The elemental composition was determined using EDX [83, 84]. The percentage of Ag metal in the present study was found to be appreciable. The EDX analysis showed the percentage relative composition of Au signal of the AuNPs with 48.08%. The other elements served as capping organic agents bound to the surface of the AuNPs [85]. This recognition was made because of the registered energy, which is characteristic of AuNPs. [86] reported the biosynthesis and characterization of AuNPs using extracts of *Tamarindus indica* L leaves are in good accordance with the results of the present study.

Oxidative stress has been linked to the cause of many deadly diseases such as Neurological disorder, Parkinson disease, mild cognitive impairment, and aging, etc the managing of which is costly [87]. Thus, plant extracts and NPs with antioxidant, antidiabetic, and anticholinesterase properties will be greatly beneficial [88]. Antioxidants are substances that can inhibit or delay the oxidation of a substrate when present in low concentrations. Due to the relationship of oxidative stress to other diseases, we, therefore, investigated the antioxidant capacities of HH extract, and the corresponding HH-AuNPs. Five essays; Ferric reducing antioxidant power, AmmoniuM Molybdate, DPPH, H_2O_2, and ABTS were carried out. The mechanism with which ferric reducing operates is known as single electron transfer (SET), whereby an antioxidant transfers an electron to the corresponding cation, which would neutralize it [89]. Thus the reducing capacity of AuNPs might be due to their quick electron transferring ability, which makes AuNPs suitable for biosensors [90].

In the present study, strong ferric reducing activities were exhibited by HH-AuNPs (77.2 ± 0.014% with IC_{50} 95.17 ± 0.025μg/mL) as compared to HH extract (55.2 ± 0.035% with 151 ± 0.13 μg/mL IC_{50}) and $HAuCl_4.3H_2O$ solution (16.92 ± 0.014 with IC_{50} = 0), while lower scavenging then ascorbic acid (84.4 ± 0.016% with IC_{50} = 79 ± 0.06 μg/mL). This inhibition is due to the HH extract hydroxyl groups attached to aromatic rings, which will perfectly participate in oxidation during the process. It is well known that phenolics have strong antioxidant activities [91]. However, since the ferric reducing mechanism is by electron transfer, the hydroxyl groups of the HH extract might be interacting with the NPs, thereby limiting the site for the oxidation process. High activities in close ranges were demonstrated for AuNPs in ferric reducing assay which might be due to the size, shape, and the surrounding environment of NPs. Therefore, it is expected that AuNPs behave somewhat differently since the smaller sized particles have a

higher surface area. Previously, NPs with smaller-sizes were reported to show enhanced activity in comparison to relatively plant extract [59].

Ammonium molybdate is an ammonium salt composed of ammonium and molybdate ions. It has a role as a poison as it contains a Molybdate. It can be used as a free radical in the antioxidant assay. In the present study, all the four samples of $HAuCl_4.3H_2O$ solution, HH extract, HH-AuNPs, and ascorbic acid were tested for their Ammonium Molybdate scavenging; $HAuCl_4.3H_2O$ solution, HH extract, HH-AuNPs, and ascorbic acid showed maximum scavenging potential of 22 ± 0.0014, 62.1 ± 0.0021, 74.3 ± 0.021, and 88.8 ± 0.001% at 160 µg/mL. The calculated IC_{50} values were found to be 91.48 ± 0.13 for HH extract, 58.5 ± 0.051 for HH-AuNPs, and 48 ± 0.11 µg/mL for ascorbic acid respectively; while the $HAuCl_4.3H_2O$ solution does not cause 50% scavenging. The scavenging potential of HH-AuNPs is higher as compared to $HAuCl_4.3H_2O$ solution and HH extract [92].

DPPH is a free radical which changes its color from violet to yellow on reduction by a hydrogen or electron [93]. In the DPPH scavenging assay, the compounds which can reduce DPPH are considered antioxidants. By DPPH radical scavenging assay, it was found that AuNPs were able to react with free oxygen radicals and hence, possessed strong antioxidant activity as compared to HH extract and $HAuCl_4.3H_2O$ solution ($HAuCl_4.3H_2O$ solution of 21 ± 0.007, HH extract 55 ± 0.059, HH AuNPs 58.6 ± 0.51, and Ascorbic acid 90 ± 0.0014% % at 160µg/mL). The biological activity of NPs is depending upon the aspect ratio of particles. NPs with a high aspect ratio have been demonstrated to exhibit good antioxidant properties [94]. The result was also confirmed by the finding of [92, 95] who showed that a higher concentration of AuNPs significantly showed high scavenging capacity as compared to *Acinetobacter* sp. Similar results were also reported by [96, 97].

H_2O_2 is an unstable inorganic compound that damages the cell membrane in the living organism. It is also known as oxidant or dioxide and can be used as free radicals in antioxidant activity. An anti-oxidant compound donates an electron to H_2O_2 ions and thus neutralizes it to water [93]. In the present study synthesized HH-AuNPs were able to scavenge 62 ± 0.041% using 160 µg/mL concentrations in comparison to $HAuCl_4.3H_2O$ solution and HH extract which scavenge 21 ± 0.021 and 56.6 ± 0.0021% respectively. The calculated IC_{50} values were found to be 136 ± 0.21 for HH extract, 105.66 ± 0.062 for HH-AuNPs, and 51.18 ± 0.3 µg/mL for ascorbic acid. [97] reported that AuNPs can catalyze the rapid decomposition of H_2O_2. H_2O_2 scavenging activity shown by AuNPs is almost equal to other embedded 3,6-dihydroxyflavone AuNPs, used to enhance the antioxidant activity (Medhe et al., 2014).

On the other hand, a clear trend can be observed for the ABTS assay. This is probably because of the difference in the mechanism of operation between the assays. ABTS is largely operating on hydrogen atom transfer. The trend in the ABTS results is such that individual AuNPs demonstrated better antioxidant capacity relative to their respective precursors. Recent research reports [19, 91, 98] supported the above submission. AuNPs biosynthesized from *Halymenia dilatata* also demonstrated higher antioxidant activity than the starting plant extract [99]. Thus biosynthesis of NPs, has been reported for

its antioxidant capacity [100]. These antioxidant compounds might get adsorbed onto the active surface of NPs. The surface reaction phenomenon of these biosynthesized NPs (due to adsorbed antioxidant moiety onto the surface) and the high surface area to volume ratio of NPs generate a tendency to interact and scavenge the free radical [101]. NPs donate electrons to free radicals due to which the free radical becomes stable. The enhanced potential of the HH-AuNPs is due to their control size, shape, and type due to which they became more reactive as compared to the plant extract [92].

Dietary antioxidants have been hypothesized to have a protective effect against α-amylase. The human salivary α-amylase digests the starch into small fragments with two or three pieces. Hence, the inhibition of the α-amylase enzyme could control the carbohydrate metabolism which also decreases the amount of glucose absorption. It seems plausible that a sufficient intake of antioxidants plays an important role in protection against type 2 diabetes [102]. In the present study the observed inhibitory percentage of α-amylase by $HAuCl_4.3H_2O$ solution, HH extract, HH-AuNPs, and standard drug Glucophage are shown. The α-amylase inhibitory activity of HH-AuNPs exhibited the highest inhibitory activity with 56 ± 0.003 µg/mL IC_{50} when compared to $HAuCl_4.3H_2O$ solution and HH extract. The positive control Glucophage has revealed the potent α-amylase inhibitory activity with the IC_{50} value of 37 ± 0.13 µg/mL. This behavior is similar to that reported by [21], therefore, closely related behaviors in the same experimental conditions are obvious. Accordingly, the improved antidiabetic performance of AuNPs over their precursor extracts has been reported by [103, 104]. The IC_{50} values of α-amylase of HH-AuNPs form also showed improved activity in agreement with previous studies [103]. The inhibiting powers of the nanomaterials may be a function of size and shape. In our results, HH-AuNPs had a size of 10.72 nm. These values are similar to the size of AuNPs in previous investigations [21]. Similarly, [105] affirmed that spherical AuNPs of sizes 20 and 40 nm in diameter induced the west Nile virus better than those of other sizes and shapes. This may be the reason for the improved enzymatic activity of AuNPs. The enzyme kinetics competitively revealed inhibition for HH on α-amylase (K_m is increased, whereas V_{max} remains the same). These findings indicate that some of the α-amylase inhibitory components in HH extract may be structural analogs of the substrate that compete for binding at the active site of α-amylase, while in the case of HH-AuNPs effect on α-amylase a non-competitive type of inhibition was reported (*Km* remained constant and V_{max} is decreased), this suggests that some of the α-amylase inhibitory components in this HH-AuNPs resulting from HH extract bind only to the enzyme-substrate complex and may alter the active site of the enzyme. α-amylase inhibitors delay the rate of carbohydrate digestion, thereby providing an alternative therapeutic option for modulation of postprandial hyperglycemia [106]. In diabetic patients with a sustained reduction of hyperglycemia is shown to decrease the risk of developing microvascular and macrovascular diseases and their associated complications [107]. The HH extract exhibited higher inhibitory activity towards the α-amylase as opposed to many other hypoglycemic plants reported in previous studies [108]. In comparison, the first time *in vitro* hypoglycemic assessment of HH-AuNPs indicates higher bioactive properties. The enhanced activity of AuNPs obtained in the α-amylase assessment may be due to their high surface area to volume ratio, thus increasing the surface area phenomenon (promoting the electron transfer reaction) and may increase the pharmacokinetics from a biological view. The effects of oral hypoglycemic drugs depend on several pharmacokinetic factors such

as absorption, metabolism, and excretion, and the actions of drugs begin inside the cells, it is believed that AuNPs' small size is easily carried across the cell membrane by transport proteins and may exhibit prolonged effects in bio-systems [109]. Given the α-amylase inhibitory effects of HH-AuNPs, the results obtained in this study are coherent with previous studies [110].

Antioxidants such as vitamin C and vitamin E have been associated with AChE inhibition and play an important role in AD treatment [102] and patients with AD on take high doses of antioxidants will have a slow cognitive deterioration rate [111]. Inhibition of the AChE is considered promising in AD disease treatment and various researches are focused on new inhibitors from the herbal resources [27, 112–114]. To our knowledge, no attention has been given to AuNPs synthesized using the plant for the treatment of AD. The $HAuCl_4.3H_2O$ solution, HH extract, and HH-AuNPs synthesized using the HH extract were screened for their in vitro AChE inhibitory activity. Their IC_{50} values are found to be 19.1 ± 0.021 for HH extract and 16.66 ± 0.011 µg/mL for HH-AuNPs while no concentration of $HAuCl_4.3H_2O$ solution cause 50% inhibition of AChE. Under the same conditions, the IC_{50} values of HH-AuNPs showed a remarkable increase in activity toward AChE than extract. This finding is noteworthy because AD is associated with AChE deficiency and AuNPs could be potential new AChE inhibitors [85]. The good anti-AChE potential of AuNPs as compared to HH extract is due to the size and shape that may find useful in the AD treatment [115]. According to Line Weaver Burk Plot HH-AuNPs causes an uncompetitive type of inhibition of AChE (both K_m and V_{max} decrease), while HH extract caused a non-competitive type of inhibition. From the kinetic study, it is reported that AuNPs primarily cause the inhibition by interaction or adsorption with the AChE enzyme. The exact mechanism by which AuNPs inhibit AChE remains unknown. The binding affinity of NPs to AChE might be due to the lipophilicity of the NPs and the hydrophobicity of the enzyme environment in ChE molecules. Another possible mechanism of AChE inhibition might be due to the adsorption of AChE on the surface of NPs resulting in conformational changes, and surface coverage leading to the inactivation of the enzyme as reported by [116]. Inactivation of the enzyme by NPs depends on physicochemical properties like shape, size, curvature, and surface functional groups. [12] proposed that inhibition by NPs is primarily caused by adsorption or interaction with AChE protein and partly by dissolved metal ions.

5. Conclusion

In this study, an environmentally facile, compassionate, straightforward, and medicinally active phytochemical route synthesized colloidal HH-AuNPs from the HH extract an indigenous plant found in abundance in Pakistan. These HH-AuNPs were characterized by the following techniques, UV-Vis spectroscopy, FTIR, SEM, EDX, and XRD. HH-AuNPs showed excellent antioxidant and inhibitory enzymatic properties than their respective HH crude extract and $HAuCl_4.3H_2O$ salt. These observations, plus evidence of their potent antioxidant and enzymatic activity from active molecules rich plants such as HH indicate the value of further studies. Thus, the synthesis of AuNPs based drugs with greater targeted activity combined with medicinal phytochemicals derived from the HH extract may result in

unprecedented opportunities directed at the discovery of a cheaper and more beneficial therapy for oxidants, type 2 diabetes, and Alzheimer's diseases

Declarations

Acknowledgments

The author wishes to thank the Higher Education Commission of Pakistan (HEC-PAK) for financial support of project No: 20-5082/NRPU/R&D/HEC.

Conflict of Interest

The authors do not have any conflict of interest regarding this article and its publication.

References

1. C.C.I. Kavitha, G. Indira, Green synthesis, characterization and antimicrobial activity of silver nanoparticles using Morindapubscens J. E. Smith root extract. J. Sci. Innov. Res. **5**(3), 83–86 (2016)
2. A. Chanda, D. Mohanta, Nanotechnology- A Potent Pharmacological Tool, International Journal of Research in Advent Technology. 46 – 16 (2016)
3. E.S. Lee, E. de Josselin de Jong, B.I. Kim, Detection of dental plaque and its potential pathogenicity using quantitative light-induced fluorescence. J. Biophotonics **12**(7), e201800414 (2019)
4. S.S. Hojjat, H. Hojjat, Effects of silver nanoparticle exposure on germination of Lentil (Lens culinaris Medik.). Int. J. Farming Allied Sci. **5**(3), 248–252 (2016)
5. S. Dubchak, A. Ogar, J.W. Mietelski, K. Turnau, Influence of silver and titanium nanoparticles on arbuscular mycorrhiza colonization and accumulation of radiocaesium in Helianthus annuus Spanish. J. Agricultural Res. **8**(1), 103–108 (2010)
6. R.K. Sastry, H.B. Rashmi, N.H. Rao, S.M. Ilyas, Integrating nanotechnology into agri-food systems research in India: a conceptual framework. Technological Forecast. Social Change **77**(4), 639–648 (2010)
7. N. Sher, M. Ahmed, N. Mushtaq, R.A. Khan, Calligonum polygonoides reduced nanosilver: A new generation of nanoproduct for medical applications. Eur. J. Integr. Med. **33**(2020), 101042 (2020)
8. S.P. Chandran, M. Chaudhary, R. Pasricha, A. Ahmad, M. Sastry, Synthesis of gold nanotriangles and silver nanoparticles using Aloe vera plant extract. Biotechnol. Prog **22**(2), 577–583 (2006)
9. P. Espitia, N. Soares, J. Coimbra, N. Andrade, R. Cruz, E. Medeiros, Zinc Oxide Nanoparticles: Synthesis, Antimicrobial Activity and Food Packaging Applications, Food and Bioprocess Technology. **5**(5), 1447–1464 (2012)
10. P.K. Jain, X. Huang, I.H. El-Sayed, M.A. El-Sayed, Noble metals on the nanoscale: Optical and photothermal properties and some applications in imaging, sensing, biology, and medicine. Acc. Chem. Res. **41**(12), 1578–1586 (2008)

11. K.N. Thakkar, S.S. Mhatre, R.Y. Parikh, Biological synthesis of metallic nanoparticles. Nanomedicine. **6**(2), 257–262 (2010)
12. Y. Wang, X. He, K. Wang, X. Zhang, W. Tan, Barbated Skullcup herb extract-mediated biosynthesis of gold nanoparticles and its primary application in electrochemistry. Colloids Surf. B Biointerfaces **73**(1), 75–79 (2009)
13. C. Dipankar, S. Murugan, The green synthesis, characterization and evaluation of the biological activities of silver nanoparticles synthesized from Iresine herbstii leaf aqueous extracts, Colloids Surf B Biointerfaces. **98**112-119 (2012)
14. S. Pandey, G. Oza, A. Mewada, M. Sharon, Green synthesis of highly stable gold nanoparticles using Momordica charantia as nano fabricator. Arch. Appl. Sci. Res. **4**(2), 1135–1141 (2012)
15. G. Sathishkumar, C. Gobinath, K. Karpagam, V. Hemamalini, K. Premkumar, S. Sivaramakrishnan, Phyto-synthesis of silver nanoscale particles using Morinda citrifolia L. and its inhibitory activity against human pathogens, Colloids Surf B Biointerfaces. **95**235-40 (2012)
16. D.R. Bhumkar, H.M. Joshi, M. Sastry, V.B. Pokharkar, Chitosan reduced gold nanoparticles as novel carriers for transmucosal delivery of insulin. Pharm. Res. **24**(8), 1415–1426 (2007)
17. K. Dubey, B.G. Anand, R. Badhwar, G. Bagler, P.N. Navya, H.K. Daima, K. Kar, Tyrosine- and tryptophan-coated gold nanoparticles inhibit amyloid aggregation of insulin. Amino Acids. **47**(12), 2551–2560 (2015)
18. P. Sharma, R. Vijavergia, In vitro α-amylase inhibitory activity and GC-MS analysis of Petrea volubilis. Int. J. Sci. Sesearch **4**(4), 190–194 (2015)
19. M. Khoshnamvand, S. Ashtiani, C. Huo, S.P. Saeb, J. Liu, Use of Alcea rosea leaf extract for biomimetic synthesis of gold nanoparticles with innate free radical scavenging and catalytic activities, J. Mol. Struct. **1179**749-755 (2019)
20. N. Torabi, A. Nowrouzi, A. Ahadi, S. Vardasbi, B. Etesami, Green synthesis of gold nanoclusters using seed aqueous extract of Cichorium intybus L. and their characterization, SN Appl. Sci **1**981 (2019)
21. D. Benedec, I. Oniga, F. Cuibus, B. Sevastre, G. Stiufiuc, M. Duma, C.M. Lucaciu, Origanum vulgare mediated green synthesis of biocompatible gold nanoparticles simultaneously possessing plasmonic, antioxidant and antimicrobial properties. Int. J. Nanomed. **13**, 1041 (2018)
22. M. Zhaleh, A. Zangeneh, S. Goorani, N. Seydi, M.M. Zangeneh, R. Tahvilian, E. Pirabbasi, In vitro and in vivo evaluation of cytotoxicity, antioxidant, antibacterial, antifungal, and cutaneous wound healing properties of gold nanoparticles produced via a green chemistry synthesis using Gundelia tournefortii L. as a capping and reducing agent, Appl. Organomet. Chem **33**5015 (2019)
23. M.P. Patil, Y.B. Seo, H.K. Lim, G.D. Kim, Biofabrication of gold nanoparticles using Agrimonia pilosa extract and their antioxidant and cytotoxic activity Green Chem. Lett. Rev. **12**208-216 (2019)
24. M.F. Zayed, R.A. Mahfoze, S.M. El-kousy, E.A. Al-Ashkar, In-vitro antioxidant and antimicrobial activities of metal nanoparticles biosynthesized using optimized Pimpinella anisum extract, Colloid Surf. A Phys. Eng. **585**124167 (2020)

25. D.K. Lahiri, M.R. Farlow, N.H. Greig, K. Sambamurti, Current drug targets for Alzheimer's disease treatment, Drug Dev. Res. **56**267-281 (2002)
26. N.S. Perry, C. Bollen, E.K. Perry, C. Ballard, Salvia for dementia therapy: review of pharmacological activity and pilot tolerability clinical trial. Pharmacol. Biochem. Behav. **75**(3), 651–659 (2003)
27. P.K. Mukherjee, V. Kumar, M. Mal, P.J. Houghton, Acetylcholinesterase inhibitors from plants. Phytomedicine. **14**(4), 289–300 (2007)
28. M. Öztürk, Anticholinesterase and antioxidant activities of Savoury (Satureja thymbra L.) with identified major terpenes of the essential oil, Food Chem. **134**48-54 (2012)
29. P.F. Stevens, *Asparagales: Amaryllidoideae"* (Angiosperm Phylogeny Website version, 2016)
30. K. Brenzel, Norris, The New Western Garden Book: The Ultimate Gardening Guide (Sunset Western Garden Book (Paper)) Flexibound (2012)
31. Y. Wang, D. Chen, X. He, J. Shen, M. Xiong, X. Wang, D. Zhou, Z. Wei, Revealing the complex genetic structure of cultivated amaryllis (Hippeastrum hybridum) using transcriptome-derived microsatellite markers. Sci. Rep. **8**(1), 10645 (2018)
32. K.S. Prasad, N. Savithramma, Biosynthesis and Validation of Silver Nanoparticles from Nymphaea caerulea American. J. Adv. Drug Delivery **3**, 149–159 (2015)
33. R. Geethalakshmi, D.V.L. Sarada, Gold and silver nanoparticles from Trianthema decandra: synthesis, characterization, and antimicrobial properties. Int. J. Nanomedicine **7**, 5375–5384 (2012)
34. M. Oyaizu, Studies on products of browning reactions: antioxidative activities of products of browning reaction prepared from glucosamine. Jpn J. Nutr. **44**, 307–315 (1986)
35. S. Velavan, P. Arivoli, K. Mahadevan, Biological reduction of silver nanoparticles using Cassia auriculata flower extract and evaluation of their in vitro antioxidant activities. Nanoscience and Nanotechnolog. Int. J. **2**(4), 30–35 (2012)
36. W. Brand-Williams, M.E. Cuvelier, C. Berset, Use of a free radical method to evaluate antioxidant activity. Food Sci. Technol-LWT **28**, 25–30 (1995)
37. E. Pick, D. Mizel, Rapid microassays for the measurement of superoxide and hydrogen peroxide production by macrophages in culture using an automatic enzyme immunoassay reader. J. Immunol. Methods **46**(2), 211–226 (1981)
38. S. Mathew, T.E. Abraham, In vitro antioxidant activity and scavenging effects of Cinnamomum verum leaf extract assayed by different methodologies. Food Chem. Toxicol. **44**(2), 198–206 (2006)
39. Y. Kwon, E. Apostolidis, K. Shetty, Inhibitory potential of wine and tea against α-amylase and α-glucosidase for management of hyperglycemia linked to type 2 diabetes, J Food Biochem. (32), 15–31 (2006)
40. H. Ali, P.J. Houghton, A. Soumyanath, alpha-Amylase inhibitory activity of some Malaysian plants used to treat diabetes; with particular reference to Phyllanthus amarus. J. Ethnopharmacol. **107**(3), 449–455 (2006)

41. H. Lineweaver, D. Burk, The Determination of Enzyme Dissociation Constants. J. Am. Chem. Soc. **56**, 658–666 (1934)
42. B.H. Hofstee, On the evaluation of the constants Vm and KM in enzyme reactions. Science. **116**(3013), 329–331 (1952)
43. J.E. Dowd, D.S. Riggs, A comparison of estimates of michaelis-menten kinetic constants from various linear transformations, J Biol Chem. **240**863-9 (1965)
44. A. Cornish-Bowden, M.L. Cárdenas, Hexokinase and 'glucokinase' in liver metabolism. Trends Biochem. Sci. **16**(8), 281–282 (1991)
45. M. Dixon, E.C. Webb, *Enzymes* (Longmans, London, 1964)
46. M. Ahmed, J. Batista, T. Rocha, C.M. Mazzanti, W. Hassan, V.M. Morsch, Comparative study of the inhibitory effect of antidepressants on cholinesterase activity in Bungarus sindanus (krait) venom, human serum and rat striatum. J. Enzyme Inhib. Med. Chem. **23**(6), 912–917 (2008)
47. J.B. Rocha, T. Emanuelli, M.E. Pereira, Effects of early undernutrition on kinetic parameters of brain acetylcholinesterase from adult rats. Acta Neurobiol. Exp. (Wars) **53**(3), 431–437 (1993)
48. M.M. Bradford, A rapid and sensitive method for the quantitation of microgram quantities of protein utilizing the principle of protein-dye binding, Anal Biochem. **72**248-54 (1976)
49. R.G.D. Steel, J.H. Torrie, *Principles and procedures of statistics: a biometrical approach* (McGraw-Hill, New York, 1984)
50. A.K. Gupta, M. Gupta, Synthesis and surface engineering of iron oxide nanoparticles for biomedical applications. Biomaterials. **26**(18), 3995–4021 (2005)
51. J.Y. Song, B.S. Kim, Rapid biological synthesis of silver nanoparticles using plant leaf extracts. Bioprocess. and Biosystems Engineering **32**(1), 79 (2008)
52. S. Shrivastava, D. Dash, Applying Nanotechnology to Human Health: Revolution in Biomedical Sciences, Journal of Nanotechnology. **2009**1-4 (2009)
53. S.S. Shankar, A. Rai, A. Ahmad, M. Sastry, Rapid synthesis of Au, Ag, and bimetallic Au core-Ag shell nanoparticles using Neem (Azadirachta indica) leaf broth. J. Colloid Interface Sci. **275**(2), 496–502 (2004)
54. N.U. Islam, K. Jalil, M. Shahid, A. Rauf, N. Muhammad, A. Khan, M.R. Shah, M.A. Khan, Green synthesis and biological activities of gold nanoparticles functionalized with Salix alba. Arab. J. Chem. **12**(8), 2914–2925 (2019)
55. T.R. Jensen, M.D. Malinsky, C.L. Haynes, D.R.P. Van, Nanosphere lithography: Tunable localized surface plasmon resonance spectra of silver nanoparticles. J. Phys. Chem. B **104**, 10549–10556 (2000)
56. C.J. Murphy, A.M. Gole, S.E. Hunyadi, J.W. Stone, P.N. Sisco, A. Alkilany, B.E. Kinard, P. Hankins, Chemical sensing and imaging with metallic nanorods, Chem Commun (Camb). (5), 544–57 (2008)
57. M. Amin, F. Anwar, M.R. Janjua, M.A. Iqbal, U. Rashid, Green synthesis of silver nanoparticles through reduction with Solanum xanthocarpum L. berry extract: characterization, antimicrobial and urease

inhibitory activities against Helicobacter pylori. Int. J. Mol. Sci. **13**(8), 9923–9941 (2012)

58. V. Armendariz, I. Herrera, J.R. Peralta-videa, M. Jose-yacaman, H. Troiani, P. Santiago, J.L. Gardea-Torresdey, Size controlled gold nanoparticle formation by Avena sativa biomass: use of plants in nanobiotechnology. J. Nanoparticle Res. J. Recent Sci. **6**(4), 377–382 (2004)
59. B. Ajitha, Y. Ashok Kumar Reddy, P. Sreedhara, Reddy, Enhanced antimicrobial activity of silver nanoparticles with controlled particle size by pH variation, Powder Technology. **269**110-117 (2015)
60. A. Mishra, M. Kumari, S. Pandey, V. Chaudhry, K.C. Gupta, C.S. Nautiyal, Biocatalytic and antimicrobial activities of gold nanoparticles synthesized by Trichoderma sp, Bioresour Technol. **166**235-42 (2014)
61. A. Bankar, B. Joshi, A.R. Kumar, S. Zinjarde, Banana peel extract mediated synthesis of gold nanoparticles. Colloids Surf. B Biointerfaces **80**(1), 45–50 (2010)
62. P.P. Gan, S.H. Ng, Y. Huang, S.F. Li, Green synthesis of gold nanoparticles using palm oil mill effluent (POME): a low-cost and eco-friendly viable approach, Bioresour Technol. **113**132-5 (2012)
63. Y. Park, Y.N. Hong, A. Weyers, Y.S. Kim, R.J. Linhardt, Polysaccharides and phytochemicals: a natural reservoir for the green synthesis of gold and silver nanoparticles. IET Nanobiotechnol. **5**(3), 69–78 (2011)
64. W.L. Barnes, A. Dereux, T.W. Ebbesen, Surface plasmon subwavelength optics. Nature. **424**(6950), 824–830 (2003)
65. M. Sathishkumar, K. Sneha, S.W. Won, C.W. Cho, S. Kim, Y.S. Yun, Cinnamon zeylanicum bark extract and powder mediated green synthesis of nano-crystalline silver particles and its bactericidal activity. Colloids Surf. B Biointerfaces **73**(2), 332–338 (2009)
66. S.S. Shankar, A. Ahmad, M. Sastry, Geranium leaf assisted biosynthesis of silver nanoparticles. Biotechnol. Prog **19**(6), 1627–1631 (2003)
67. N. Chanda, R. Shukla, A. Zambre, S. Mekapothula, R.R. Kulkarni, K. Katti, K. Bhattacharyya, G.M. Fent, S.W. Casteel, E.J. Boote, J.A. Viator, A. Upendran, R. Kannan, K.V. Katti, An effective strategy for the synthesis of biocompatible gold nanoparticles using cinnamon phytochemicals for phantom CT imaging and photoacoustic detection of cancerous cells. Pharm. Res. **28**(2), 279–291 (2011)
68. M. Azizi, S. Sedaghat, K. Tahvildari, P. Derakhshi, A. Ghaemi, Synthesis of silver nanoparticles using Peganum harmala extract as a green route. Green Chem. Lett. Reviews **10**(4), 420–427 (2017)
69. G. Jayashree, G. Kurup Muraleedhara, S. Sudarslal, V.B. Jacob, Anti-oxidant activity of Centella asiatica on lymphoma-bearing mice. Fitoterapia. **74**(5), 431–434 (2003)
70. A. Kumar, S. Dogra, A. Prakash, Neuroprotective Effects of Centella asiatica against Intracerebroventricular Colchicine-Induced Cognitive Impairment and Oxidative Stress, Int J Alzheimers Dis. 2009(2009)
71. R.K. Das, N. Gogoi, U. Bora, Green synthesis of gold nanoparticles using Nyctanthes arbortristis flower extract. Bioprocess. Biosyst Eng. **34**(5), 615–619 (2011)

72. S. Ghosh, S. Patil, M. Ahire, R. Kitture, D.D. Gurav, A.M. Jabgunde, S. Kale, K. Pardesi, V. Shinde, J. Bellare, D.D. Dhavale, B.A. Chopade, Gnidia glauca flower extract mediated synthesis of gold nanoparticles and evaluation of its chemocatalytic potential, J Nanobiotechnology. **10**17 (2012)
73. S. Jain, M.S. Mehata, Medicinal Plant Leaf Extract and Pure Flavonoid Mediated Green Synthesis of Silver Nanoparticles and their Enhanced Antibacterial Property. Sci. Rep. **7**(1), 15867 (2017)
74. A.D. Dwivedi, K. Gopal, Biosynthesis of silver and gold nanoparticles using Chenopodium album leaf extract. Colloids Surf. Physicochem Eng Asp **369**(1–3), 27–33 (2010)
75. C. Li, D. Li, G. Wan, J. Xu, W. Hou, Facile synthesis of concentrated gold nanoparticles with low size-distribution in water: temperature and pH controls. Nanoscale Res. Lett. **6**(1), 440 (2011)
76. T. Elavazhagan, K.D. Arunachalam, Memecylon edule leaf extract mediated green synthesis of silver and gold nanoparticles, Int J Nanomedicine. **6**1265-78 (2011)
77. T.S.R. Devi, S. Gayathri, FTIR and FT-Raman spectral analysis of paclitaxel drugs. Int. J. Pharm. Sci. Rev. Res. **2**, 106–110 (2010)
78. P. Dauthal, M. Mukhopadhyay, N.M. Nanoparticles, Plant-Mediated Synthesis, Mechanistic Aspects of Synthesis, and Applications. Industrial & Engineering Chemistry Research. **55**(36), 9557–9577 (2016)
79. B. Syed, N. Bisht, S.B. Prithvi, R.N. Karthik, A. Prasad, B.L. Dhananjaya, S. Satish, H. Prasad, M.N.N. Prasad, Phytogenic synthesis of nanoparticles from Rhizophora mangle and their bactericidal potential with DNA damage activity, Nano-Structures & Nano-Objects. **10**112-115 (2017)
80. A.M. Awwad, N.M. Salem, A.O. Abdeen, Green synthesis of silver nanoparticles using carob leaf extract and its antibacterial activity. Int. J. Industrial Chem. **4**(1), 29 (2013)
81. B. Sadeghi, M. Mohammadzadeh, B. Babakhani, Green synthesis of gold nanoparticles using Stevia rebaudiana leaf extracts: Characterization and their stability. J. Photochem. Photobiol B **148**, 101–106 (2015)
82. B. Schaffer, U. Hohenester, A. Trügler, F. Hofer, High-resolution surface plasmon imaging of gold nanoparticles by energy-filtered transmission electron microscopy, Phys. Rev. B. **79**041401 (2009)
83. A.O. Dada, F.A. Adekola, E.O. Odebunmi, A novel zerovalent manganese for removal of copper ions: synthesis, characterization and adsorption studies. Appl. Water Sci. **7**(3), 1409–1427 (2017)
84. A.O. Dada, F.A. Adekola, E.O. Odebunmi, Kinetics and equilibrium models for sorption of Cu(II) onto a novel manganese nano-adsorbent. J. Dispersion Sci. Technol. **37**(1), 119–133 (2016)
85. N. Suganthy, V. Sri Ramkumar, A. Pugazhendhi, G. Benelli, G. Archunan, Biogenic synthesis of gold nanoparticles from Terminalia arjuna bark extract: assessment of safety aspects and neuroprotective potential via antioxidant, anticholinesterase, and antiamyloidogenic effects. Environ. Sci. Pollution Res. **25**(11), 10418–10433 (2018)
86. S.N. Correa, A.M. Naranjo, A.P. Herrera, Biosynthesis and characterization of gold nanoparticles using extracts of tamarindus indica L leaves, Journal of Physics: Conference Series. **687**012082 (2016)
87. L.A. Pham-Huy, H. He, C. Pham-Huy, Free Radicals, Antioxidants in Disease and Health. Int. J. Biomed. Sci. **4**(2), 89–96 (2008)

88. L. Perez-Fons, M.T. GarzÓn, V. Micol, Relationship between the antioxidant capacity and effect of rosemary (Rosmarinus officinalis L.) polyphenoLSTE on membrane phospholipid order, J. Agric. Food Chem. **58**161-171 (2009)
89. S. Duletić-Laušević, A.A. Aradski, S. Kolarević, B. Vuković-Gačić, M. Oalđe, J. Živković, K. Šavikin, P.D. Marin, Antineurodegenerative, antioxidant and antibacterial activities and phenolic components of Origanum majorana L.(Lamiaceae) extracts, J. Appl. Bot. Food Qual. **91**126-13 (2018)
90. J.J. Gooding, M.T. Alam, A. Barfidokht, L. Carter, Nanoparticle mediated electron transfer across organic layers: from current understanding to applications, J Braz Chem Soc **25**418-426 (2014)
91. S. BarathManiKanth, K. Kalishwaralal, M. Sriram, S.R.K. Pandian, H.S. Youn, S. Eom, S. Gurunathan, Anti-oxidant effect of gold nanoparticles restrains hyperglycemic conditions in diabetic mice, J. Nanobiotechnol **8**16 (2010)
92. S.B. Nadhe, S.A. Wadhwani, R. Singh, B.A. Chopade, Green Synthesis of AuNPs by Acinetobacter sp. GWRVA25: Optimization, Characterization, and Its Antioxidant Activity, Front Chem. **8**474 (2020)
93. S. Medhe, P. Bansal, M.M. Srivastava, Enhanced antioxidant activity of gold nanoparticle embedded 3,6-dihydroxyflavone: a combinational study. Appl. Nanosci. **4**(2), 153–161 (2014)
94. S. Sharma, A.K. Manhar, P.J. Bora, S.K. Dolui, M. Mandal, Evaluation of antioxidant and antibacterial activity of various aspect ratio gold (Au) nanorods, Adv. Mater. Lett. **6**235 – 241 (2015)
95. S.R. Guntur, N.S. Kumar, M.M. Hegde, V.R. Dirisala, In Vitro Studies of the Antimicrobial and Free-Radical Scavenging Potentials of Silver Nanoparticles Biosynthesized From the Extract of Desmostachya bipinnata, Anal Chem Insights. **13**1177390118782877 (2018)
96. S.A. Wadhwani, M. Gorain, P. Banerjee, U.U. Shedbalkar, R. Singh, G.C. Kundu, B.A. Chopade, Green synthesis of selenium nanoparticles using Acinetobacter sp. SW30: optimization, characterization and its anticancer activity in breast cancer cells, Int J Nanomedicine. **12**6841-6855 (2017)
97. W. He, Y.T. Zhou, W.G. Wamer, X. Hu, X. Wu, Z. Zheng, M.D. Boudreau, J.J. Yin, Intrinsic catalytic activity of Au nanoparticles with respect to hydrogen peroxide decomposition and superoxide scavenging. Biomaterials. **34**(3), 765–773 (2013)
98. J.R. Nakkala, E. Bhagat, K. Suchiang, S.R. Sadras, Comparative study of antioxidant and catalytic activity of silver and gold nanoparticles synthesized from Costus pictus leaf extract, J. Mater. Sci. Technol. **31**986-994 (2015)
99. M. Vinosha, S. Palanisamy, R. Muthukrishnan, S. Selvam, E. Kannapiran, S. You, N.M. Prabhu, Biogenic synthesis of gold nanoparticles from Halymenia dilatata for pharmaceutical applications: Antioxidant, anti-cancer and antibacterial activities. Process. Biochem. **85**, 219–229 (2019)
100. S.A.S. Chatha, A.I. Hussain, R. Asad, M. Majeed, N. Aslam, Bioactive components and antioxidant properties of Terminalia arjuna L. extracts, J Food Process Technol. **2**1 – 5 (2014)
101. P. Dauthal, M. Mukhopadhyay, In-vitro free radical scavenging activity of biosynthesized gold and silver nanoparticles using Prunus armeniaca (apricot) fruit extract, J Nanopart Res. **15**1366 (2013)
102. M. Steele, G. Stuchbury, G. Münch, The molecular basis of the prevention of Alzheimer's disease through healthy nutrition. Exp. Gerontol. **42**(1–2), 28–36 (2007)

103. S. Bisht, G. Feldmann, S. Soni, R. Ravi, C. Karikar, A. Maitra, A. Maitra, Polymeric nanoparticle-encapsulated curcumin ('nanocurcumin'): A novel strategy for human cancer therapy. J. Nanobiotechnol. **5**, 1–18 (2007)
104. S. Khaleel, K. Govindaraju, R. Manikandan, J. Seog, E. Young, G. Singaravelu, Phytochemical mediated gold nanoparticles and their PTP 1B inhibitory activity, Colloids Surf. B Biointerfaces **75**405-409 (2010)
105. P. Virk, Anti-diabetic activity of green gold-silver nanocomposite with trigonella foenum graecum l. seeds extract on streptozotocin-induced diabetic rats. Pakistan J. Zool. **50**(2), 711–718 (2018)
106. R. Subramanian, M.Z. Asmawi, A. Sadikun, In vitro alpha-glucosidase and alpha-amylase enzyme inhibitory effects of Andrographis paniculata extract and andrographolide. Acta Biochim. Pol. **55**(2), 391–398 (2008)
107. D.K. Patel, R. Kumar, D. Laloo, S. Hemalatha, Diabetes mellitus: an overview on its pharmacological aspects and reported medicinal plants having antidiabetic activity. Asian Pac. J. Trop. Biomed. **2**(5), 411–420 (2012)
108. P.K. Mukherjee, K. Maiti, K. Mukherjee, P.J. Houghton, Leads from Indian medicinal plants with hypoglycemic potentials. J. Ethnopharmacol. **106**(1), 1–28 (2006)
109. V. Karthick, V.G. Kumar, T.S. Dhas, G. Singaravelu, A.M. Sadiq, K. Govindaraju, Effect of biologically synthesized gold nanoparticles on alloxan-induced diabetic rats-an in vivo approach, Colloids Surf B Biointerfaces. **122**505-511 (2014)
110. V. Malapermal, I. Botha, S.B.N. Krishna, J.N. Mbatha, Enhancing antidiabetic and antimicrobial performance of Ocimum basilicum, and Ocimum sanctum (L.) using silver nanoparticles. Saudi J. Biol. Sci. **24**(6), 1294–1305 (2017)
111. P. Mecocci, M.C. Polidori, Antioxidant clinical trials in mild cognitive impairment and Alzheimer's disease. Biochim. Biophys. Acta **1822**(5), 631–638 (2012)
112. L.S. Schneider, Treatment of Alzheimer's disease with cholinesterase inhibitors. Clin. Geriatr. Med. **17**(2), 337–358 (2001)
113. F. Sharififar, M. Moshafi, E. Shafazand, A. Koohpayeh, Acetyl cholinesterase inhibitory, antioxidant and cytotoxic activity of three dietary medicinal plants. Food Chem. **130**, 20–23 (2012)
114. I.E. Orhan, F.S. Senol, T. Ercetin, A. Kahraman, F. Celep, G. Akaydin, B. Sener, M. Dogan, 2013. s.., , Assessment of anticholinesterase and antioxidant properties of selected sage (Salvia) species with their total phenol and flavonoid content, Ind. Crop. Prod. **41**21-30
115. N. Dorosti, F. Jamshidi, Plant-mediated gold nanoparticles by Dracocephalum kotschyi as anticholinesterase agent: Synthesis, characterization, and evaluation of anticancer and antibacterial activity. J. Appl. Biomed. **14**(3), 235–245 (2016)
116. A.A. Vertegel, R.W. Siegel, J.S. Dordick, Silica nanoparticle size influences the structure and enzymatic activity of adsorbed lysozyme Langmuir. **20**6800-6807 (2004)

Figures

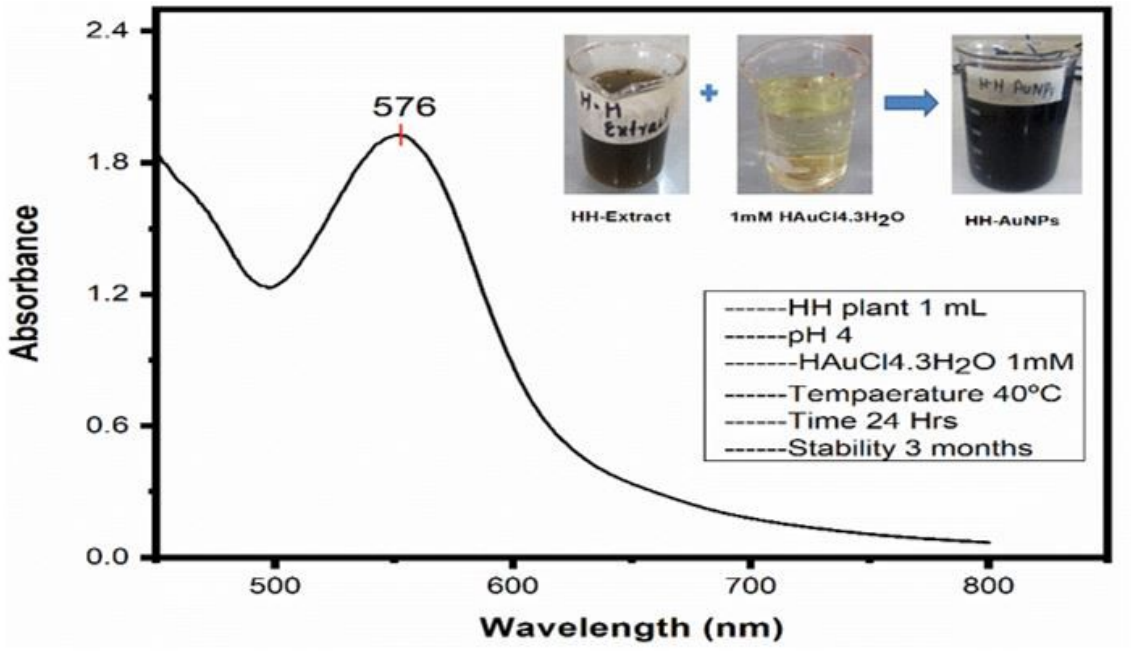

Figure 1

UV–vis absorption spectrum of HH-AuNPs.

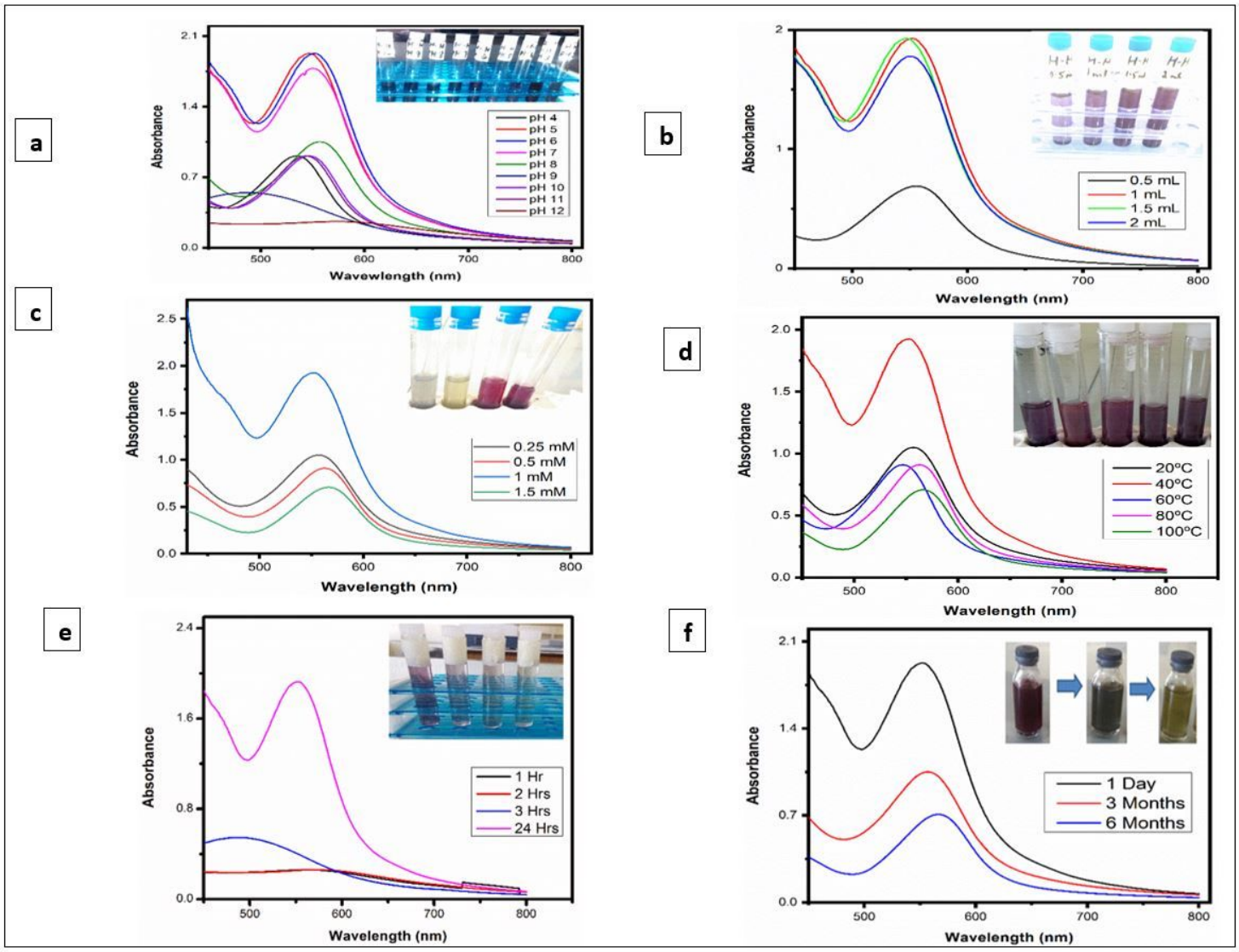

Figure 2

(2a, 2b, 2c, 2d, 2e, and 2f) UV–spectra of HH-AuNPs with different pH, $HAuCl_4.3H_2O$ salt, the volume of extract, temperature, time, and stability.

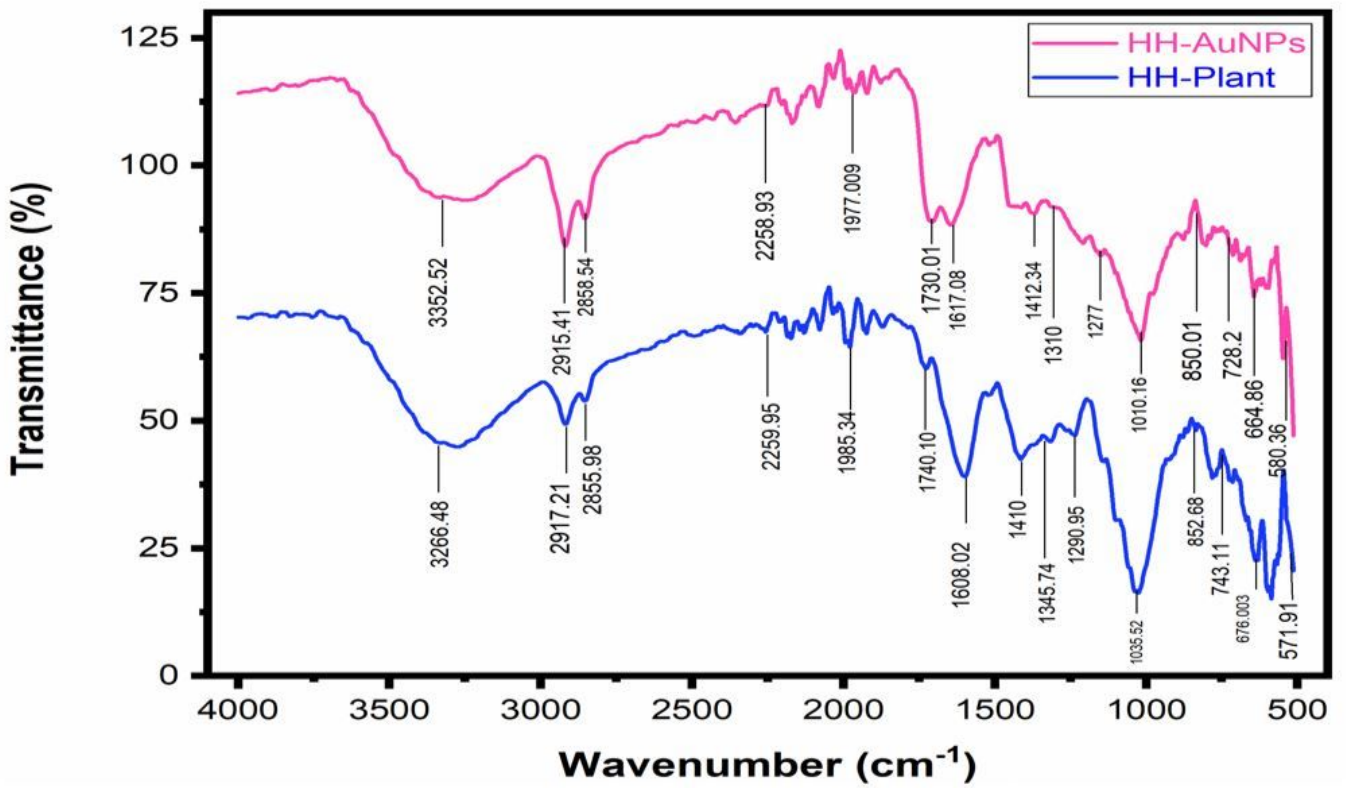

Figure 3

(3a and 3b) FT-IR analysis of HH extract and HH-AuNPs.

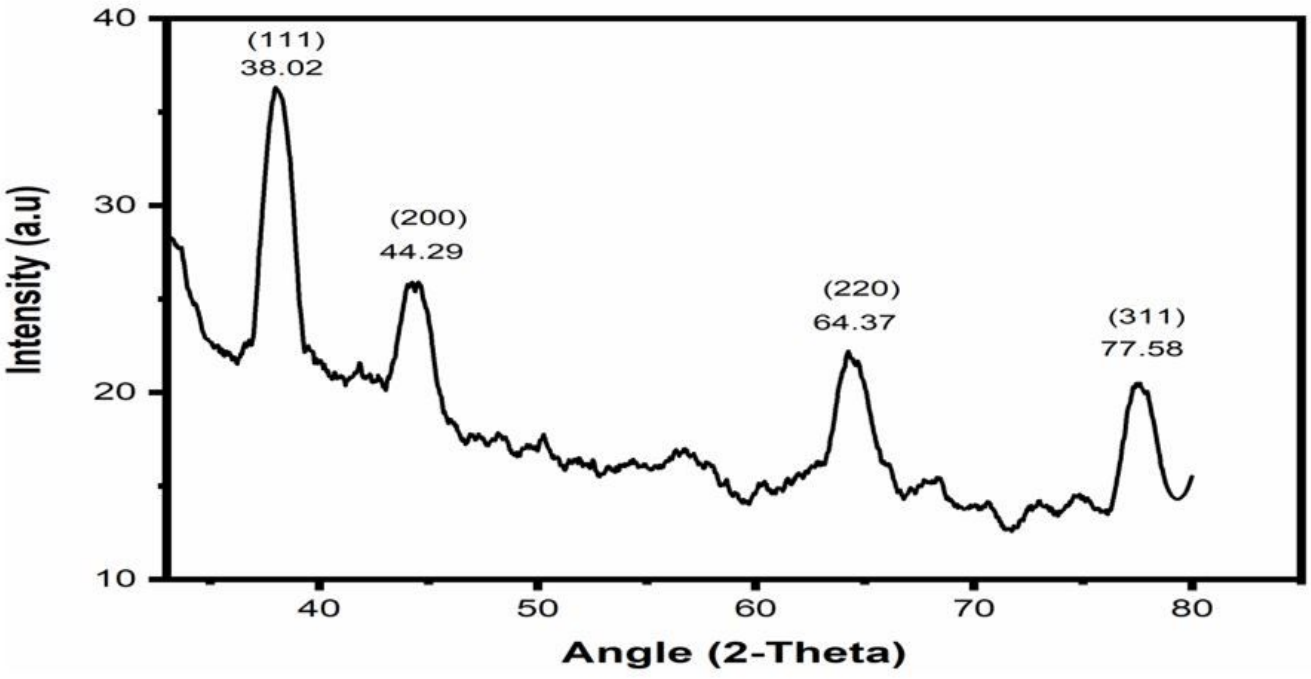

Figure 4

XRD pattern analysis of HH-induced AgNPs.

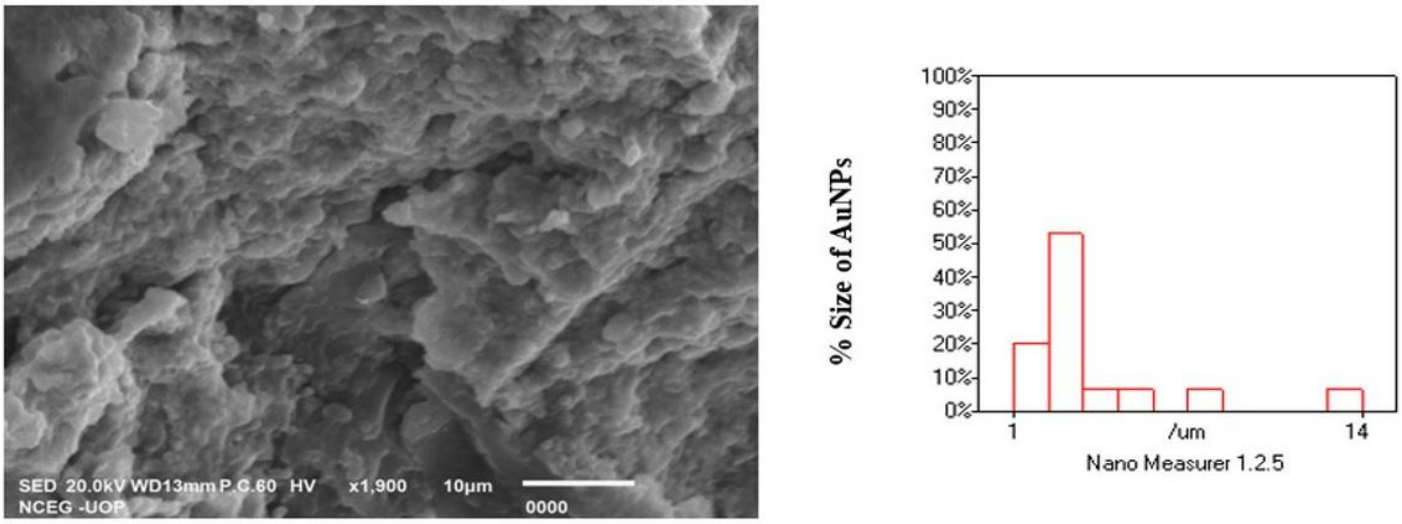

Figure 5

SEM analysis and SEM calculated the size of HH-AuNPs.

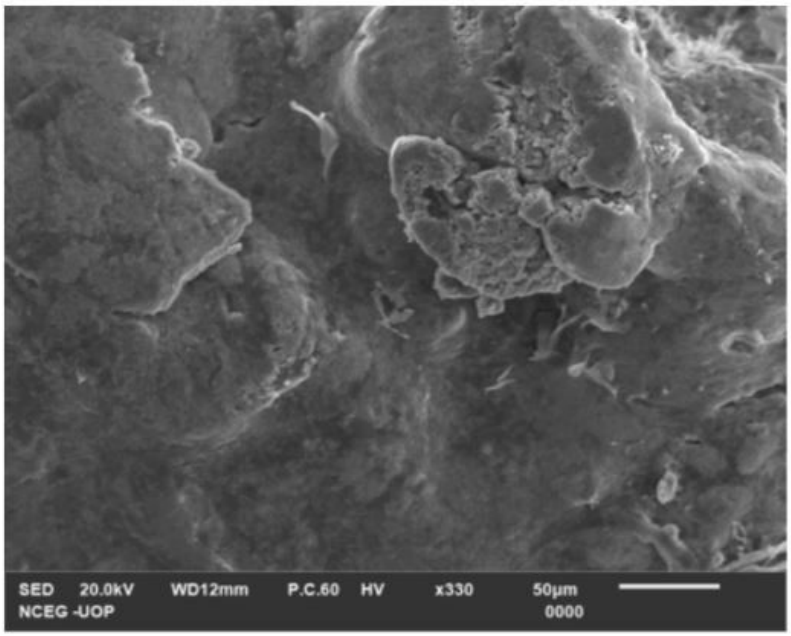

Volt : 20.00 kV
Mag. : x 330
Date : 2022/02/11
Pixel : 1280 x 960

Acquisition Condition
Instrument : IT100LA
Volt : 20.00 kV
Current : ---
Process Time : T4
Live time : 60.00 sec.
Real Time : 62.00 sec.
DeadTime : 4.00 %
Count Rate : 2288.00 CPS

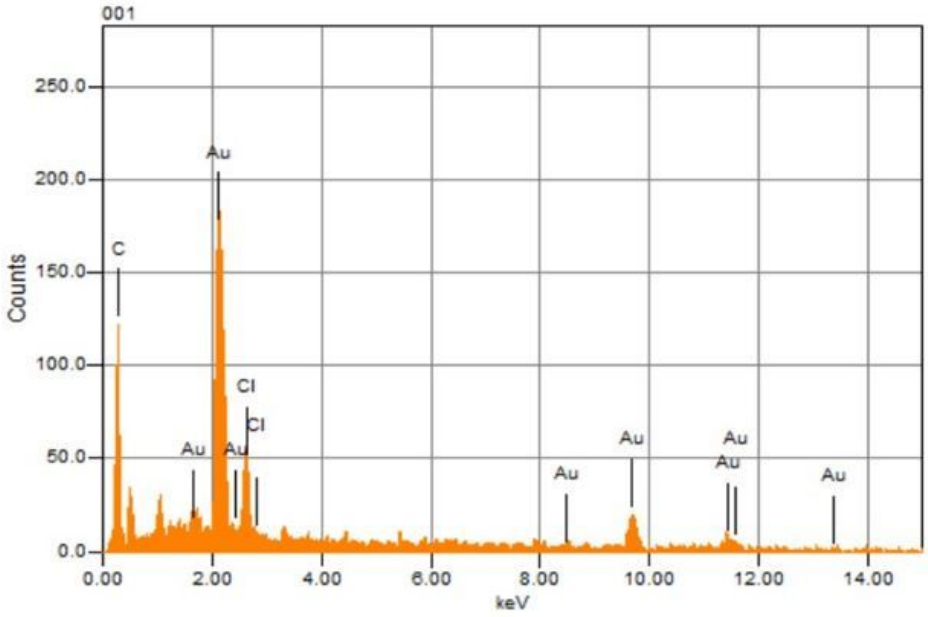

Formula	mass%	Atom%	Sigma	Net	K ratio	Line
C	46.34	90.58	0.18	2777	0.0003503	K
Cl	5.58	3.69	0.18	2148	0.0004693	K
Au	48.08	5.73	0.85	12261	0.0040879	M
Total	100.00	100.00				

Figure 6

EDX analysis of HH-AuNPs.

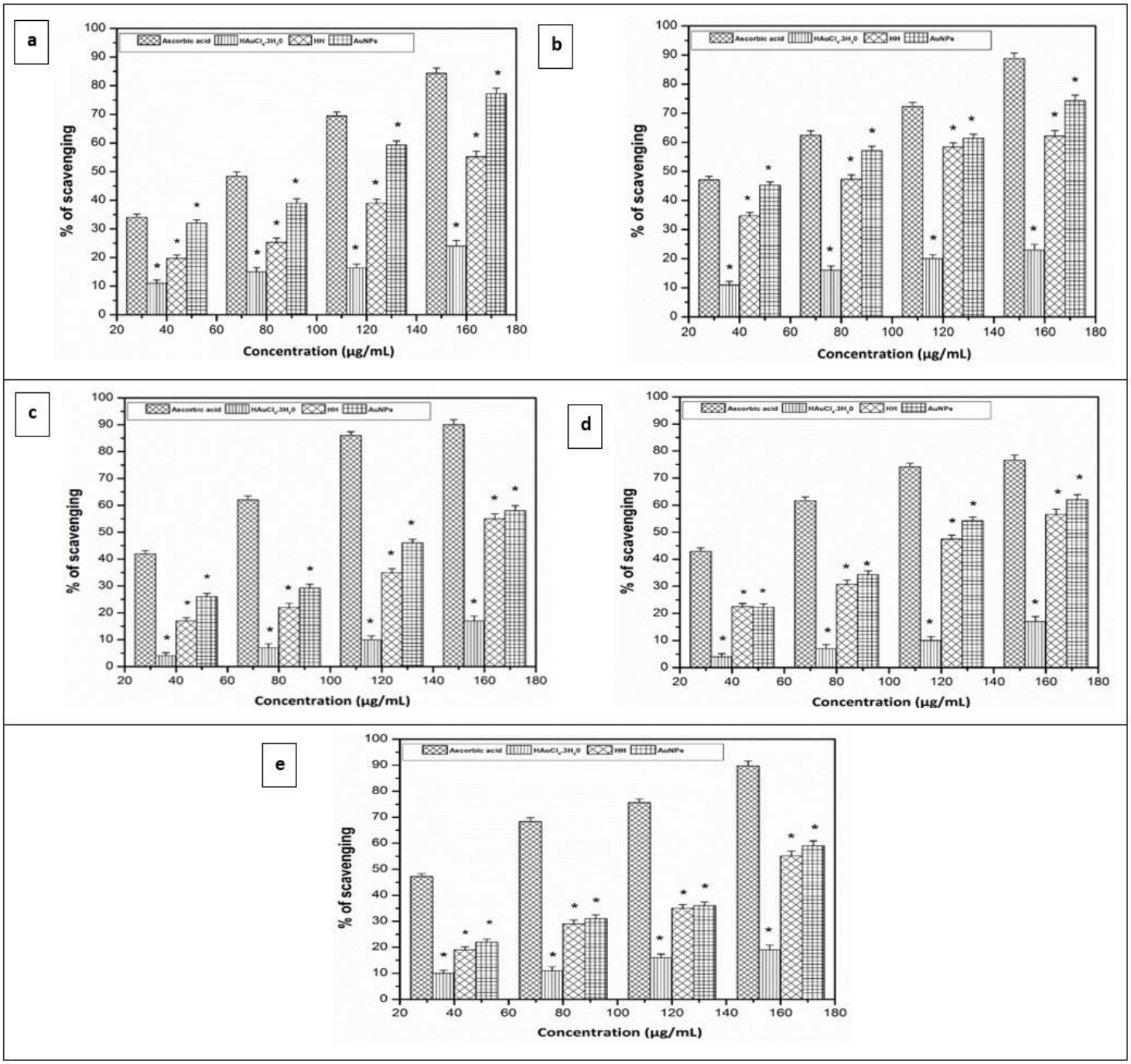

Figure 7

(7a, 7b, 7c, 7d, and 7e) Ferric reducing power assay (7A), Ammonium molybdenum (7B), DPPH scavenging (7C), H_2O_2 inhibition activity (7D), and ABTS scavenging potential (7E) of $HAuCl_4.3H_2O$ salt, HH extract, and HH-AuNPs. Data are expressed as mean ± standard deviation (SD; n = 3).

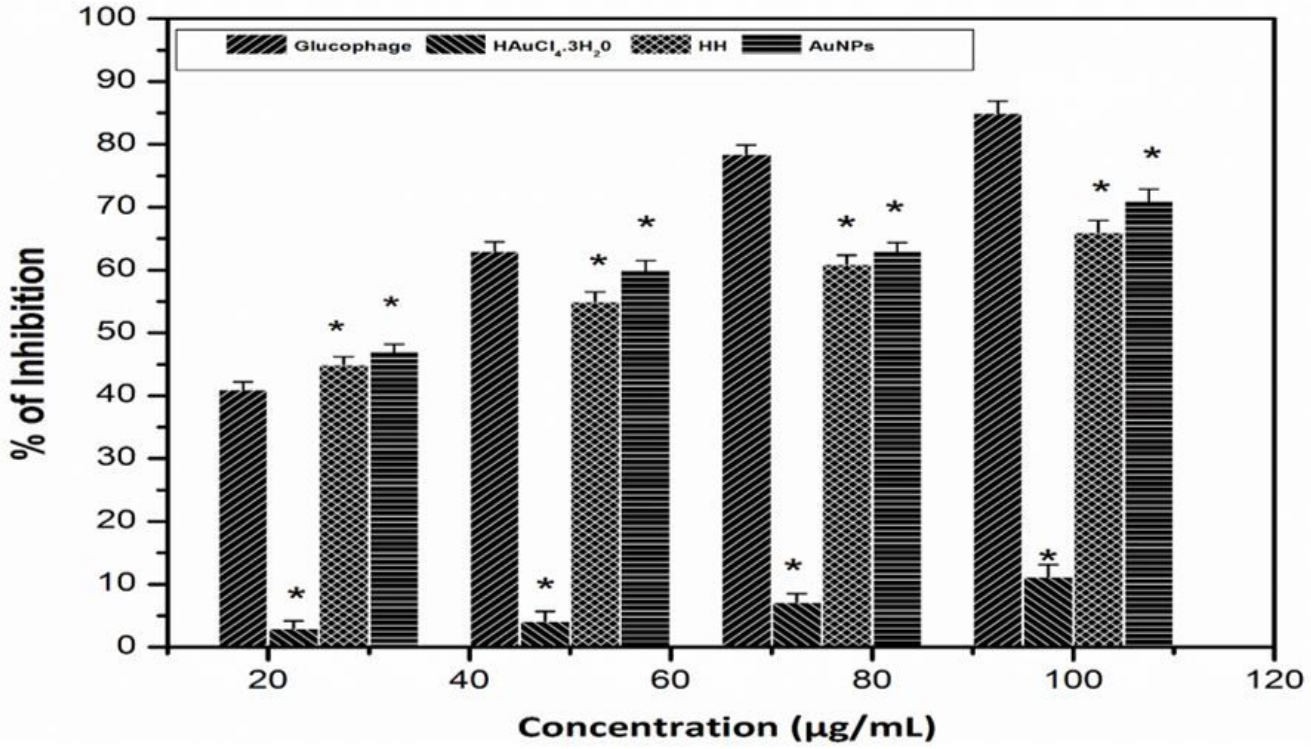

Figure 8

In vitro α-amylase Inhibitory activity of HH-AuNPs, HH extract, and Glucophage. Data are expressed as mean ± standard deviation (SD; n = 2).

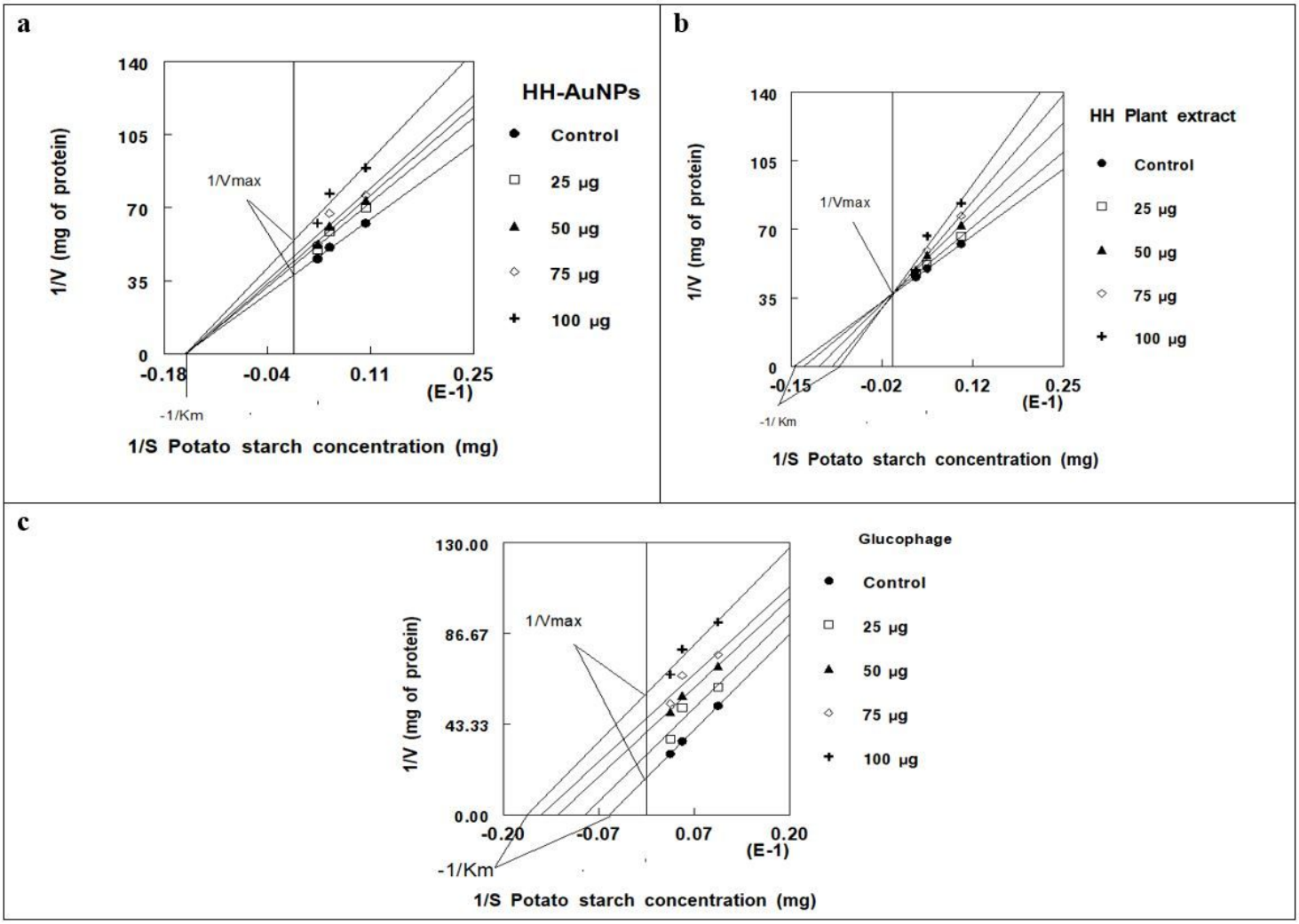

Figure 9

(9a, 9b, and 9c) HH-AuNPs caused non-competitive (K_m constant and V_{max} decrease), HH extract caused competitive type of inhibition (K_m increase and V_{max} remain constant), while Glucophage cause an uncompetitive type of inhibition (both K_m and V_{max} decrease). Data are expressed in the form of Lineweaver–Burk (reciprocal of enzyme velocity versus reciprocal of potato starch) plot. The results represent the mean of three different experiments done in triplicate by using different concentrations of extract as shown in the legend boxes.

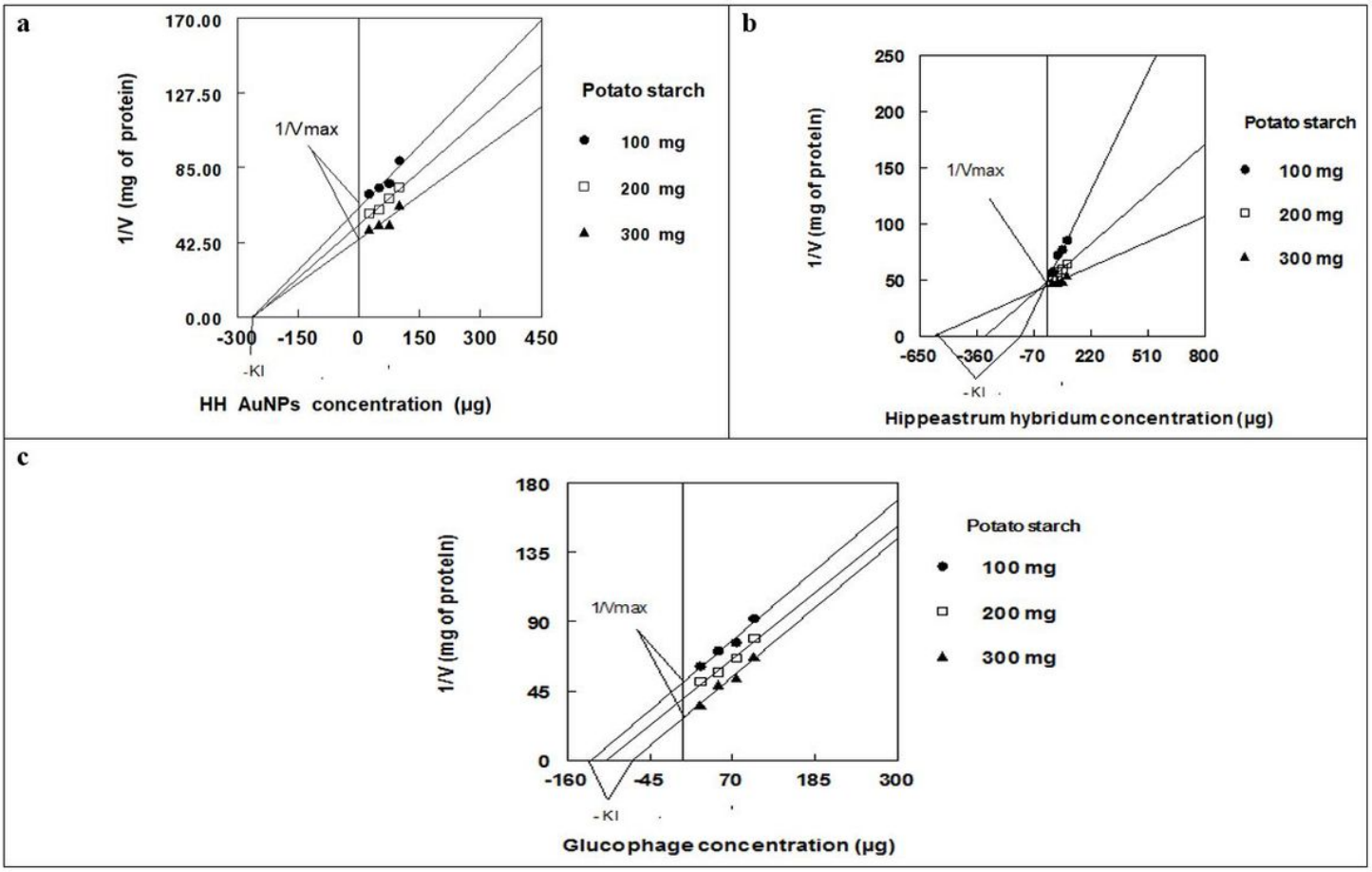

Figure 10

(10a, 10b, and 10c) The $V_{maxiapp}$ and K_{lapp} were determined for HH-AuNPs, HH extract, and Glucophage from Dixon plots for α-amylase. The $V_{maxiapp}$ is equal to the reciprocal of the y-axis intersection of each line for each potato starch concentration while K_{lapp} is equal to the x-axis intersection in the Dixon plot.

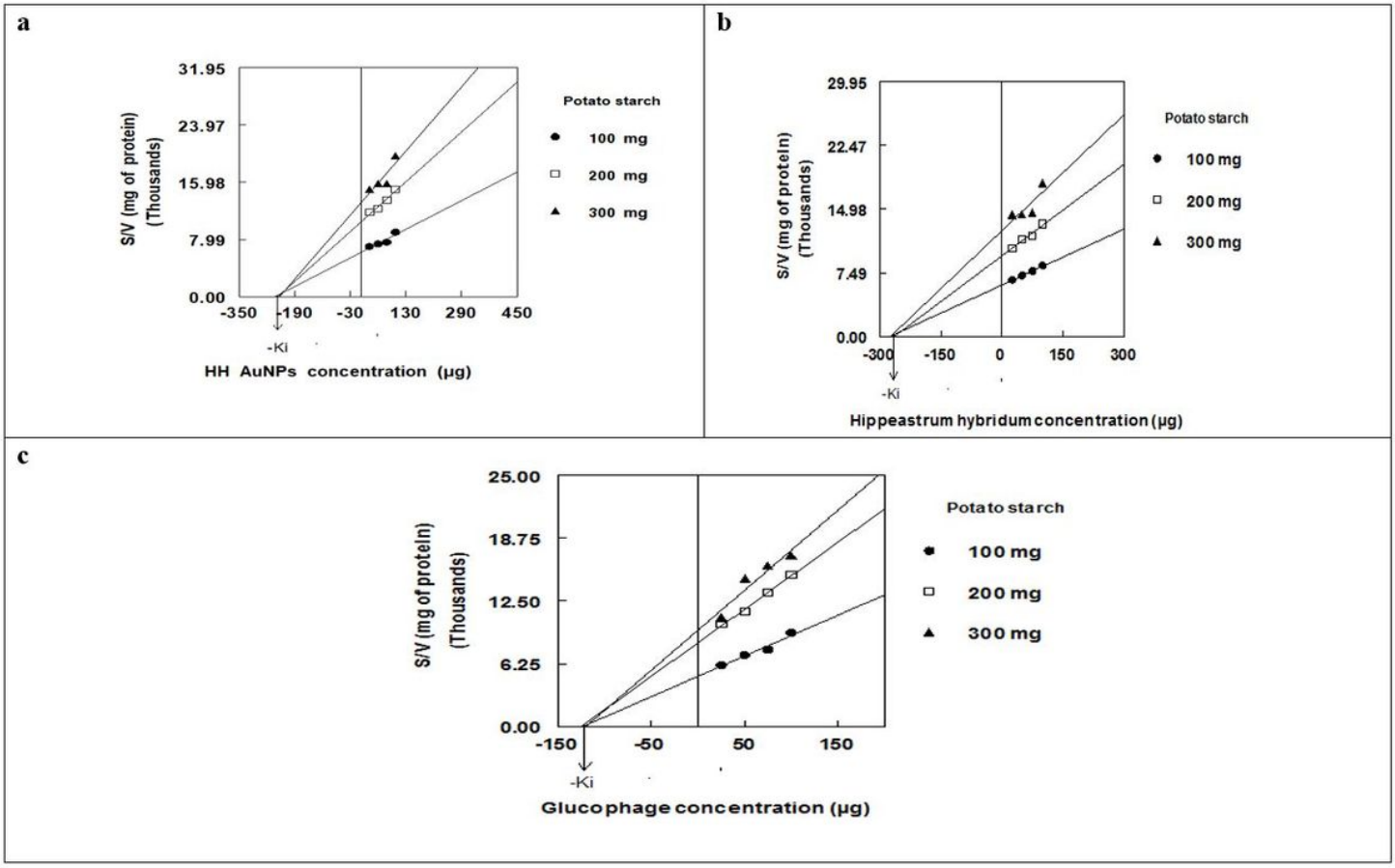

Figure 11

(11a, 11b, and 11c) The K_i (inhibition constant) was obtained for α-amylase using the Cornish-Bowden plot of S/V vs. [I].

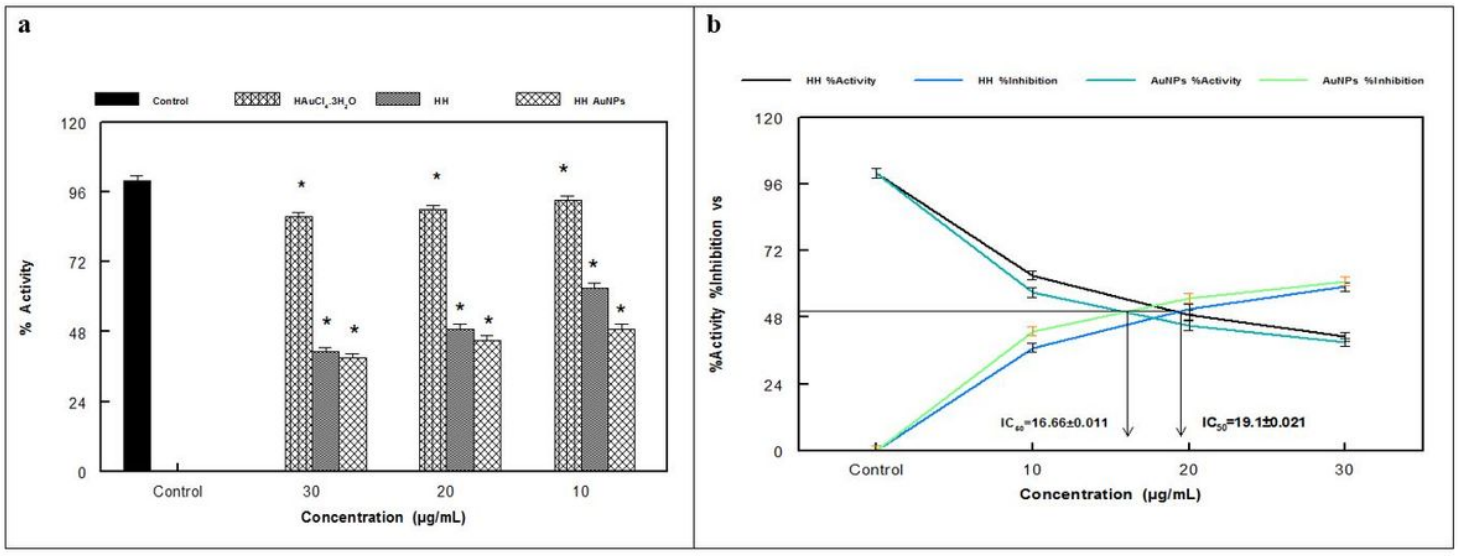

Figure 12

Inhibition of AChE in the presence and absence of HH-AuNPs and HH extract in the dose-dependent mode was measured at 421 nm by using fixed 0.5 mM ACh concentration with 50 mM phosphate buffer (pH 7.4) and 10 mM DTNB in 1 mL assay which were preincubated for 10 min before ACh addition. The experiments were repeated three times; the obtained results were similar in all three cases and significantly different from the control. * P < 0.05.

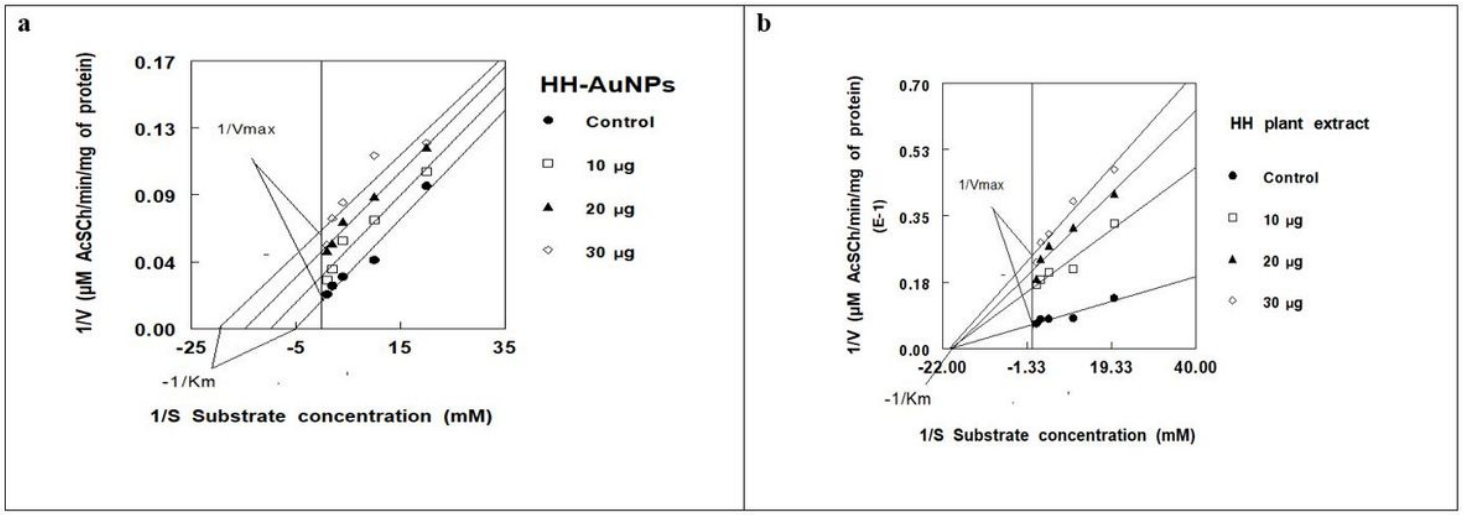

Figure 13

(13a and 13b) Both HH-AuNPs and HH extract caused a non-competitive type of inhibition (K_m remain constant and V_{max} decrease) of krait snake venom AChE. Data are expressed in the form of Lineweaver–Burk (reciprocal of enzyme velocity versus reciprocal of AcSCh) plot. The results represent the mean of three different experiments done in triplicate by using different concentrations of HH extract.

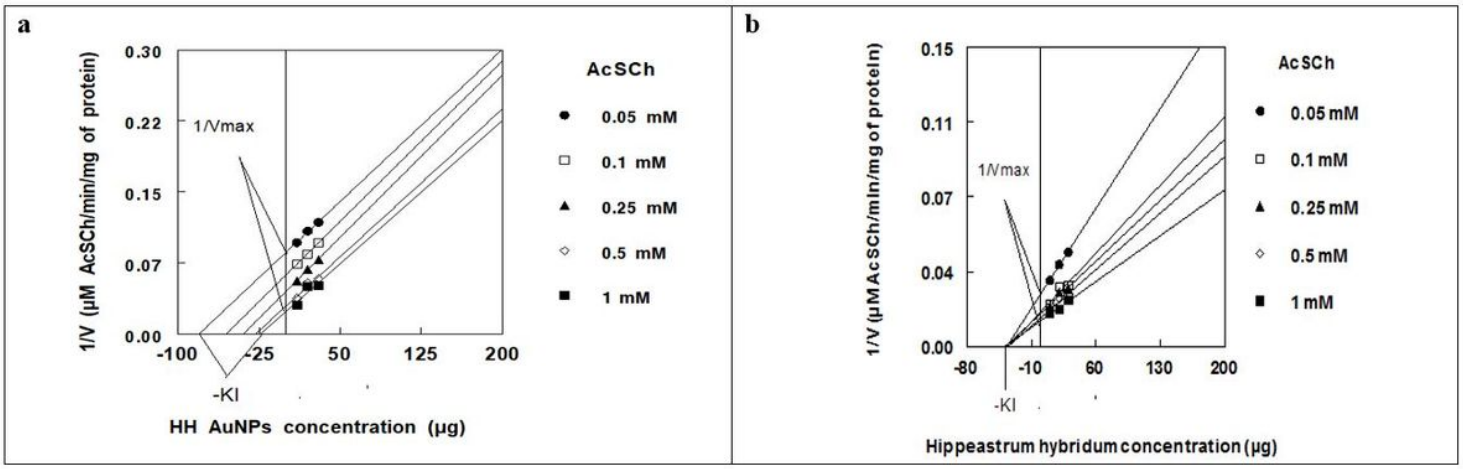

Figure 14

(14a and 14b) The $V_{maxiapp}$ and K_{Iapp} for both HH-AuNPs and HH extract were determined from Dixon plots for AChE. The $V_{maxiapp}$ is equal to the reciprocal of the y-axis intersection of each line for each AcSCh concentration while K_{Iapp} is equal to the x-axis intersection in the Dixon plot.

Figure 15

(15a and 15b) The K_i (inhibition constant) was obtained for AChE using the Cornish-Bowden plot of S/V vs. [I] for both HH-AuNPs and HH extract.